



# BEL-Float

## Topic 1 - Operational & towing performance

Deliverable 1 - Dataset containing the results of numerical simulations (motions, forces) of the operational performance analysis

Date of delivery: 08/11/2024

**Author:** Ir. Ajie Brama Krishna Pribadi

**Review:** Ir. Marc Mansuy, Prof. Dr. Ir. Evert Lataire

**University:** Ghent University

**Faculty:** Faculty of Engineering and Architecture

**Department:** Department of Civil Engineering

**Research Group:** Ships and Marine Technology



*Financially supported by the FPS Economy (FOD Economie) under the call 2022 of the Energy Transition Fund.*



# Contents

<b>1</b>	<b>Introduction</b>	<b>2</b>
1.1	Objective of the deliverable . . . . .	2
1.2	Reference floating offshore wind turbine platform . . . . .	2
1.3	Simulation tool and numerical model setup . . . . .	3
1.4	Coordinate systems . . . . .	4
<b>2</b>	<b>Verification study</b>	<b>8</b>
2.1	Decay tests . . . . .	8
2.2	Regular and irregular waves . . . . .	12
2.3	Wind and waves combination . . . . .	14
<b>3</b>	<b>Simulation matrix</b>	<b>16</b>
<b>4</b>	<b>Selective results and discussion</b>	<b>17</b>
4.1	Influence of second order wave forces . . . . .	17
4.2	Influence of wave period . . . . .	23
4.3	Damaged scenario . . . . .	25
<b>5</b>	<b>Concluding remarks</b>	<b>28</b>
	<b>References</b>	<b>30</b>

# 1 Introduction

## 1.1 Objective of the deliverable

This report serves as a complementary document to the deliverable 1.1.1.1 (D1.1.1.1): Dataset containing the results of numerical simulations (motions, forces) of the operational performance analysis. The dataset contains the numerical simulation output of a reference Floating Offshore Wind Turbine (FOWT) performed for various wind and wave conditions. This serves as input to the other tasks shown in Figure 1, namely Topic 3, Topic 5 and Topic 6 of the BEL-Float project to which different numerical tools will be developed by other research groups (OWI-lab, 2024). Additionally, the output is also made publicly accessible for those interested in developing their own numerical tools and/or reduced-order models. Figure 1 shows the flow of the output to the different research topics of BEL-Float and a public repository. The dataset comprises a total of 1152 different simulation cases, with 384 regular waves cases and 768 irregular waves cases. Each simulation contains 783 different OpenFAST outputs. The dataset is divided into 9 sub-datasets and 1 repository storing the parent input files. This dataset is stored in Zenodo platform and can be downloaded from the following hyperlinks: [part 1](#), [part 2](#), [part 3](#), [part 4](#), [part 5](#), [part 6](#), [part 7](#), [part 8](#), [part 9](#) and [parent input files](#).

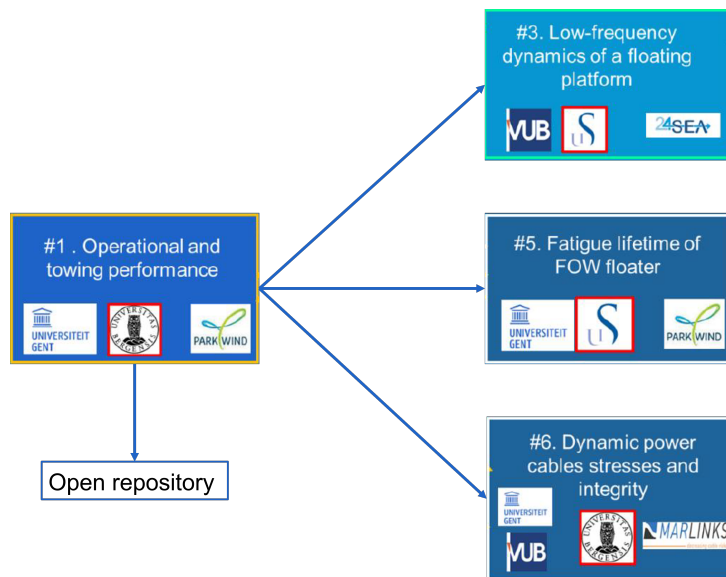


Figure 1: Flowchart of D1.1.1.1 output from Topic 1.

## 1.2 Reference floating offshore wind turbine platform

The offshore code comparison collaboration continuation (OC4) semi-submersible developed by the DeepCwind consortium is used as a reference FOWT platform for this study. This reference platform is chosen because of its robustness in terms of data availability and studies that have been performed over a decade by various researchers (Goupee, Koo, Lambrakos, & Kimball, 2012; Goupee, Fowler, Kimball, Helder, & de Ridder, 2014; A. Robertson, Jonkman, Vorpahl, et al., 2014; A. N. Robertson et al., 2017, 2020; Hall & Goupee, 2015; A. Pribadi, Donatini, Lataire, Fernandez, & Martínez-Estévez, 2022). The platform properties and detailed design specification can be found in (A. Robertson, Jonkman, Masciola, et al., 2014). Consequently, as the

aforementioned report indicated, the OC4 platform is paired with the 5-MW NREL turbine to which the specification is defined in (A. Robertson, Jonkman, Masciola, et al., 2014). Figure 3 shows the visualization of the reference FOWT platform used for the analysis performed in this report.

### 1.3 Simulation tool and numerical model setup

To conduct the numerical simulations performed in this report, an open-source aero-servo-hydro-elastic numerical tool called [OpenFAST](#) v3.5.3 (B. Jonkman et al., 2024) is utilized. OpenFAST contains different modules that handle different aspects necessary to simulate a floating offshore wind turbine system. The modules used in this study are shown in Figure 2. In addition to the software/modules specified in Figure 2, TurbSim (B. J. Jonkman, 2014) is used to generate a turbulent wind field as the input to the InflowWind module. Additionally, a boundary element method (BEM) solver is necessary to obtain the hydrodynamic coefficients and wave excitation force in the frequency domain, which must follow the WAMIT (WAMIT, Inc., 2023) output format. The original OpenFAST source code (v3.5.3) was adapted to obtain additional output of Morison drag on cylindrical element members. By default, the user can specify only up to 9 Morison members output. Considering that the DeepCwind OC4 platform has 16 submerged cylindrical members, a modification to the source was made to accommodate the possibility of getting the Morison drag output for up to 16 members. This output is a necessary input for the numerical modeling performed in [Topic 5](#). The adaptation to the OpenFAST code by author of this report is stored as a forked to the original OpenFAST GitHub repository (A. B. K. Pribadi, 2024). The OpenFAST input used for the simulations performed in this study is taken and adapted from the numerical model published in OpenFAST r-test GitHub repository (OpenFAST, 2024b). This numerical model uses WAMIT output to calculate the impulse response function (IRF) (Cummins, 1962) and wave excitation force in HydroDyn. Additionally, this publicly-accessible DeepCwind OC4 OpenFAST model (OpenFAST, 2024b) includes WAMIT output .12s and .12d which are the total second order forces of sum- and difference- frequency, respectively. Thus, the simulations performed in this report includes the contribution of second order wave forces as the importance was previously studied in (Bayati, Jonkman, Robertson, & Platt, 2014). Furthermore, a hybrid approach is used. In this case, the wave excitation and radiation forces are calculated using the potential flow theory whereas viscous drag is included using the drag term of the Morison equation (Morison, O'Brien, Johnson, & Schaaf, 1950). The importance of using the hybrid approach to model the hydrodynamics of the DeepCwind OC4 FOWT platform has been studied extensively in (A. Robertson, Jonkman, Masciola, et al., 2014; Wendt, Robertson, Jonkman, & Hayman, 2015). The main particulars of the whole system can be found in (A. Robertson, Jonkman, Masciola, et al., 2014) to which the OpenFAST setup files can be downloaded from (OpenFAST, 2024b).

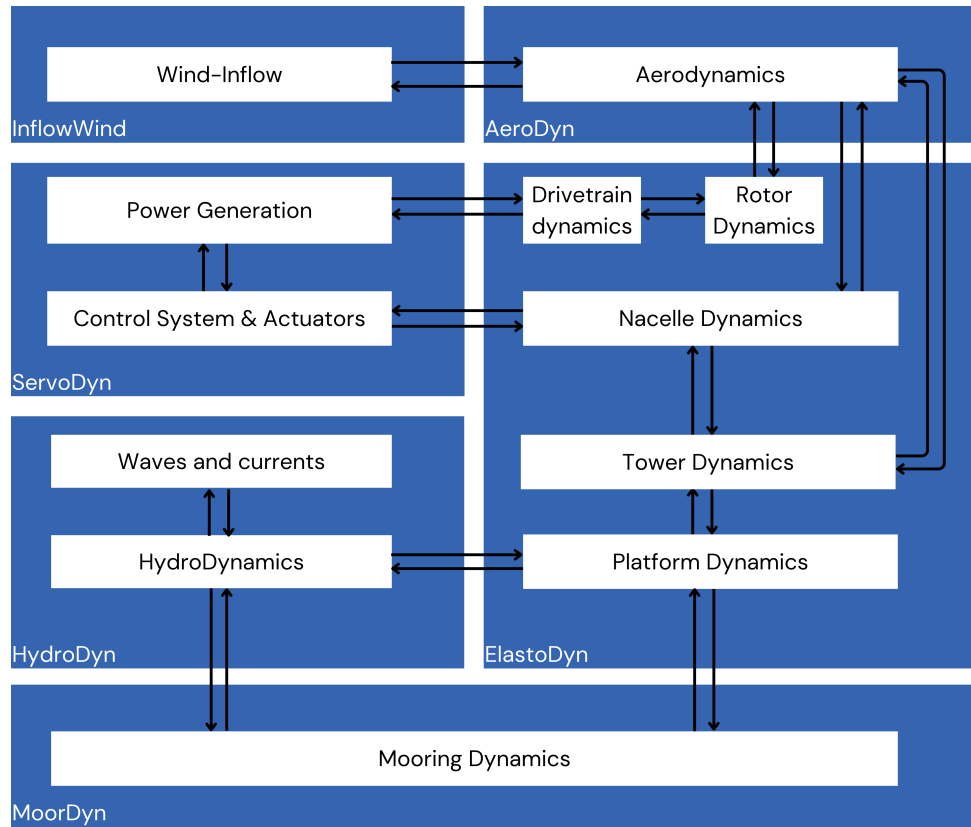


Figure 2: Flowchart of OpenFAST modules used in this study, adapted from (J. Jonkman et al., 2020).

## 1.4 Coordinate systems

### 1.4.1 Global inertial frame

The global inertial frame in OpenFAST sets the origin (0,0,0) horizontally coincide with the undisplaced position of the center line of the tower and vertically at the mean sea level (MSL) (J. M. Jonkman & Buhl, 2005). Figure 3 shows the 3D view of the location of the origin of the global coordinate system with respect to the undisplaced position of the platform. The origin of the global coordinate system in the XZ and YZ plan views are shown in Figure 4 and Figure 5. The platform's motions are defined with respect to the origin as follows:

- Surge: translation along x-axis, positive towards x-axis
- Sway: translation along y-axis, positive towards y-axis
- Heave: translation along z-axis, positive towards z-axis
- Roll: rotation around x-axis, positive counter-clockwise about x-axis
- Pitch: rotation around y-axis, positive counter-clockwise about y-axis
- Yaw: rotation around z-axis, positive counter-clockwise about z-axis

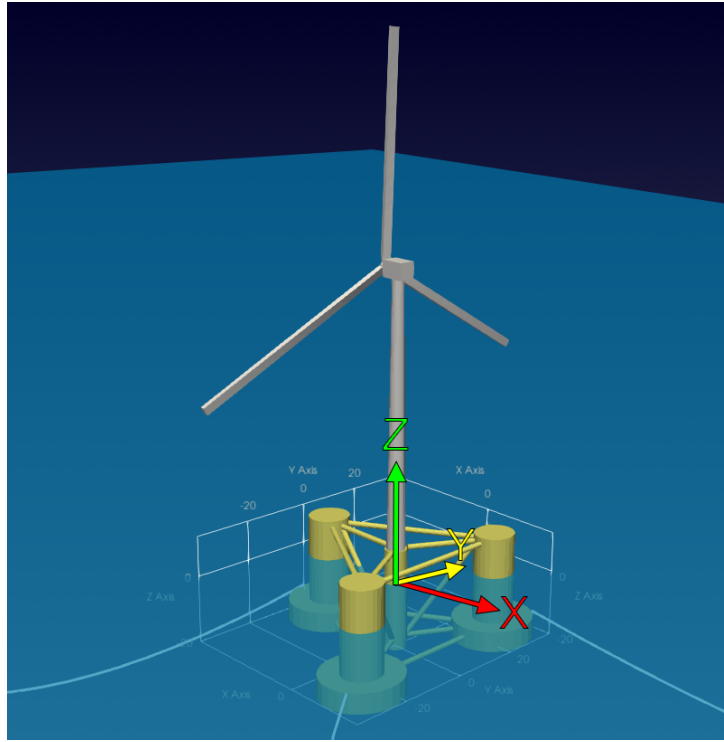


Figure 3: OC4 deepwind reference FOWT platform.

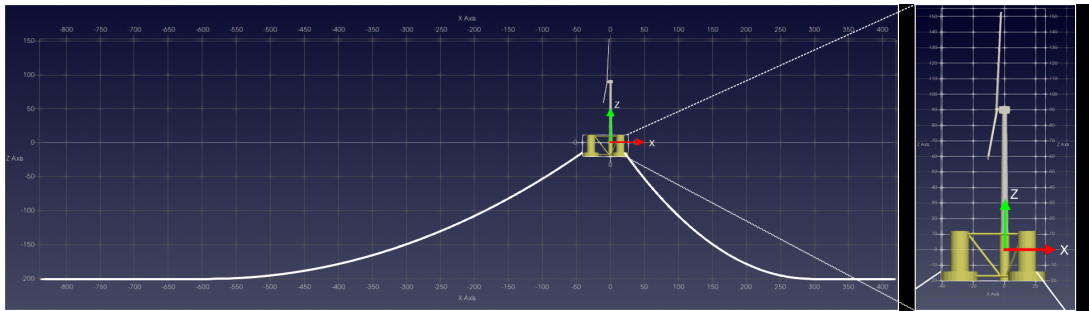


Figure 4: FOWT platform mooring configuration in XZ view.

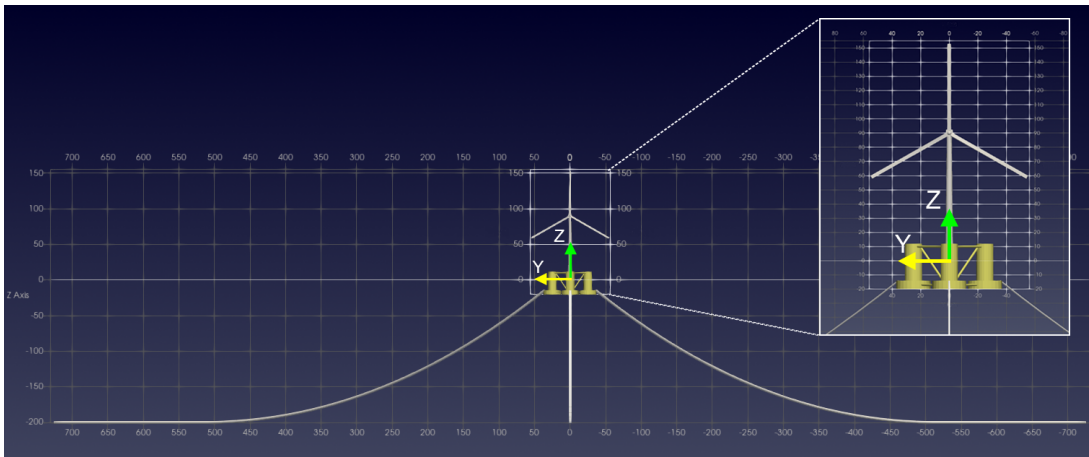


Figure 5: FOWT platform mooring configuration in YZ view.

### 1.4.2 Wind direction and InflowWind coordinate system

The InflowWind module follows the meteorological wind direction with the rotation angle around z-axis increasing clockwise. This may seem counter-intuitive as it is the opposite direction to the right handed coordinate system used in the global inertial frame defined in Subsection 1.4.1. Propagation direction 0 degree means that the wind is coming from negative x-axis and propagating to the positive x-axis, shown in Figure 6. Following the meteorological rotation angle, 45.0 degree means that the wind is coming from negative x-axis and positive y-axis, and propagating to the positive x-axis and negative y-axis, shown in Figure 7. Further explanation regarding InflowWind coordinate system and convention can be found in (Platt, Jonkman, & Jonkman, 2016). The nacelle are set to always face the direction of the incoming wind. The initial position for the simulation of 0 degree and 45.0 degree wind direction are shown in Figure 6 and Figure 7, respectively.

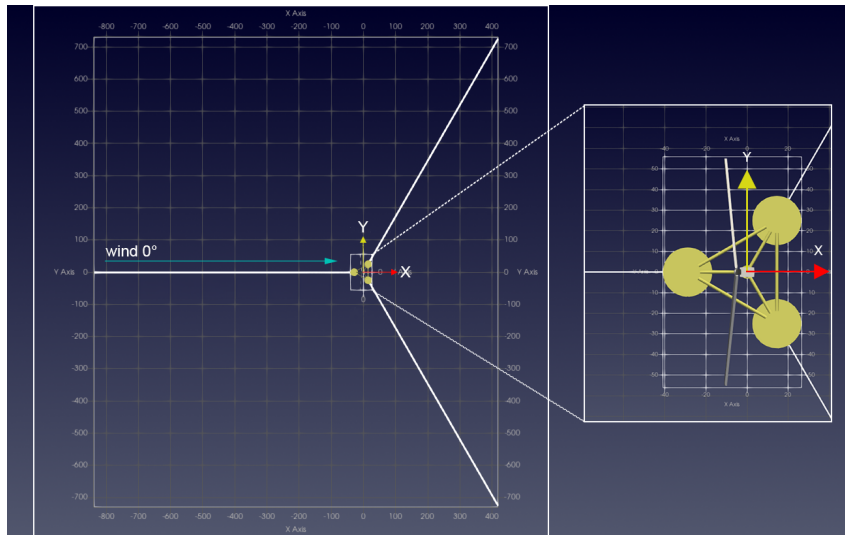


Figure 6: 0 degree wind direction in XY plan view.

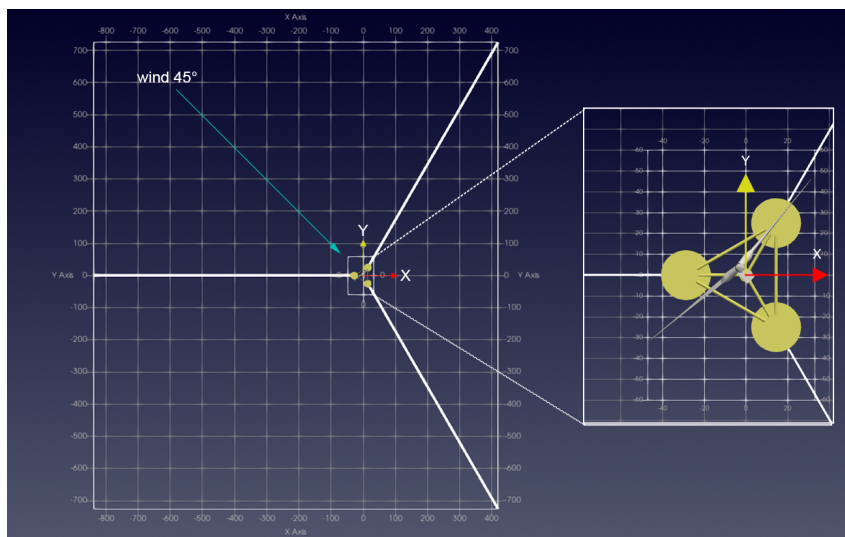


Figure 7: 45.0 degree wind direction in XY plan view. Note that the nacelle is oriented perpendicular to the wind direction.

### 1.4.3 Wave direction and HydroDyn coordinate system

In this study, only wave heading of 0 degree is considered, which corresponds to the wave propagating towards the positive x axis, as shown in Figure 8. Further details of the coordinate system and convention used in HydroDyn can be found in (J. M. Jonkman, Robertson, & Hayman, 2014). All output channels of HydroDyn module are with respect to the global coordinate system, described in 1.4.1.

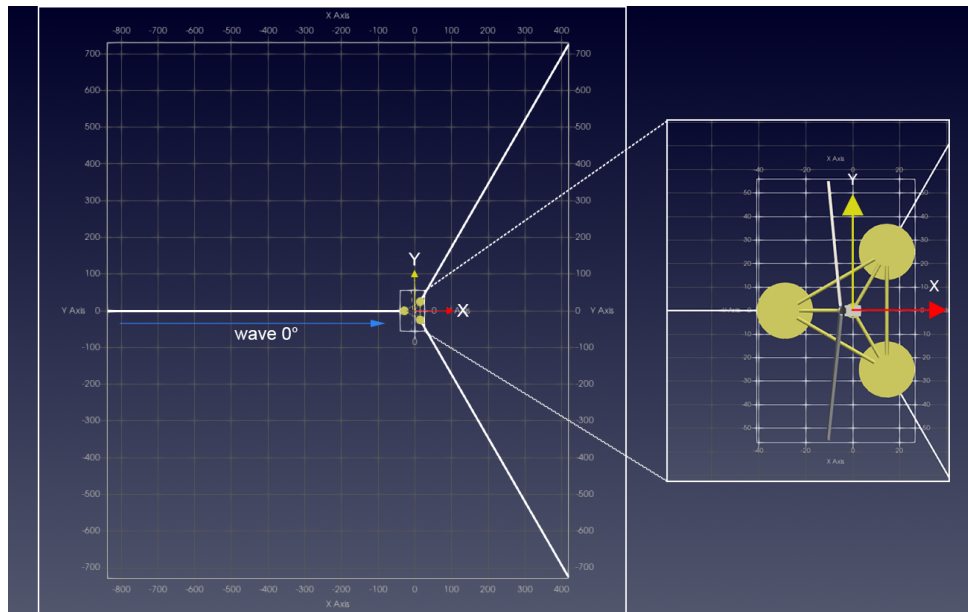


Figure 8: 0 degree wave direction in XY plan view.

### 1.4.4 Other coordinate systems

Although this study focuses on the hydrodynamics of the platform, other outputs corresponding to the aerodynamics, structural dynamics, and other aspects of a floating offshore wind turbine system are included in the dataset. Each module may have their own coordinate system and for that the reader is referred to the manual of the respective module, which can be found in (OpenFAST, 2024a). For convenience, OpenFAST provides a documentation to which the transformation between different coordinate systems is defined (J. M. Jonkman, 2005).

## 2 Verification study

To verify that the OpenFAST model is correctly setup, a comparison is made for the selective Load Cases (LCs) against the DeepCwind OC4 benchmark study in (A. Robertson, Jonkman, Vorpahl, et al., 2014). The complete dataset from their numerical benchmark study can be downloaded from [an open repository](#) (International Energy Agency, 2024). For this comparison, only the results from the DeepLines WT and OrcaFlex software are included. In essence, only non-quasi-static mooring numerical models are compared since MoorDyn v2.0 (Hall, 2020) used in OpenFAST is a dynamic mooring solver. The selective LCs are summarized in Table 1.

Table 1: Selective Load Cases (LCs) performed for the verification study against (A. Robertson, Jonkman, Vorpahl, et al., 2014)

LC	Description	Wind condition	Wave condition
1.3a	Surge decay test	-	-
1.3b	Heave decay test	-	-
1.3c	Pitch decay test	-	-
2.1	Regular waves	-	H=6.0 m; T=10.0 s
2.2	Irregular waves	-	JONSWAP $\gamma=2.87$ ; Hs=6.0 m; Tp=10.0 s
3.1	Wind and waves	Steady, $V_{hub}=8.0$ m/s	H=6.0 m; T=10.0 s

### 2.1 Decay tests

Surge decay test was performed by setting the x position of the platform at +20.0 m from the origin. Despite the slight amplitude deviation, the natural period derived from the surge motion in this study is similar to the benchmark results, which is 111.0 s (frequency of 0.009 Hz). In general, a good agreement is found in the surge between this study and the DeepLines WT software in terms of motion and fairlead tension, shown in Figure 9 and Figure 10. In the same manner, the heave decay test is performed by putting an offset of the platform only in the z-axis (vertical position). In this case, the platform is set to be at 6.0 m above the mean sea level. As shown in Figure 11, good agreement is found between all codes to which all converged to the same heave natural period of 17.6 s (frequency of 0.056 Hz). In terms of fairlead tension, all codes give varying results in the transient region. However, they all eventually converge to the same tension that is 1100.0 kN, shown in Figure 12.

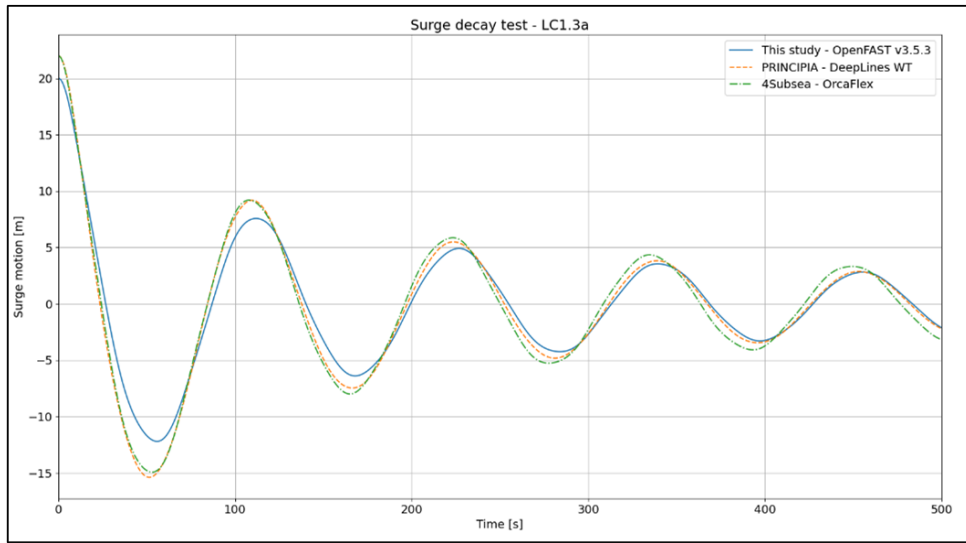


Figure 9: Surge motion on LC 1.3a surge decay test

Lastly, the pitch decay test was done by setting an initial pitch of 8.0 degrees. This results in the pitch natural period of 25.0 s (frequency of 0.04 Hz), albeit the pitch motion of this study deviates from other codes after the transient region. However, the fairlead tension agrees with the OrcaFlex results. The deviation in heave and pitch can be attributed to the hydrodynamic modeling of the heave disk. There are 3 heave disks in the DeepCwind OC4 platform to which they contribute by adding extra damping to the system. In OpenFAST, this is modeled using the Morison equation in the axial direction (toward the z-axis). However, fine-tuning is needed to obtain the axial drag coefficient that represents the behavior of the platform due to the presence of the heave disk. For this study, the axial drag coefficient follows the one derived in (Wendt et al., 2015). Overall, the natural periods simulated in this study show good agreement with the experimental data. The comparisons are summarized in Table 2.

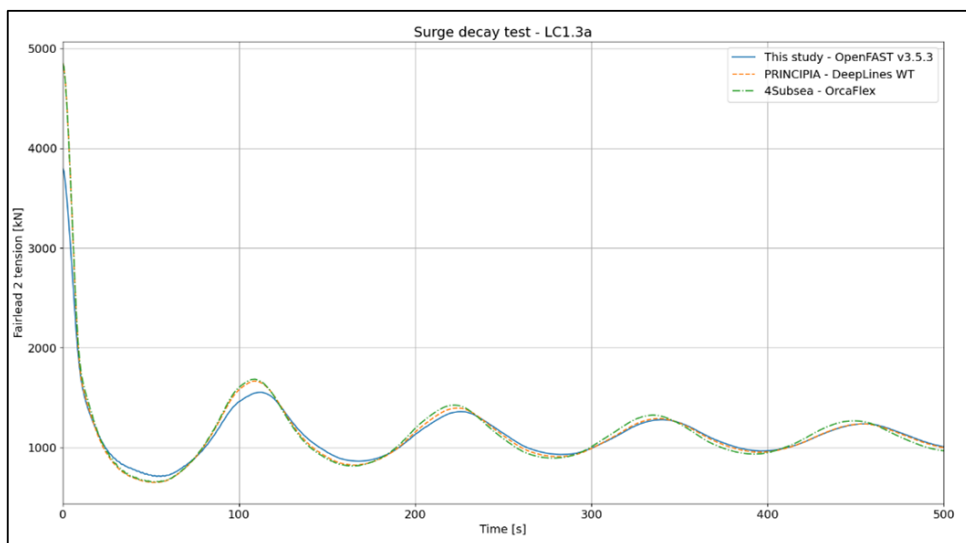


Figure 10: Fairlead tension on LC 1.3a surge decay test

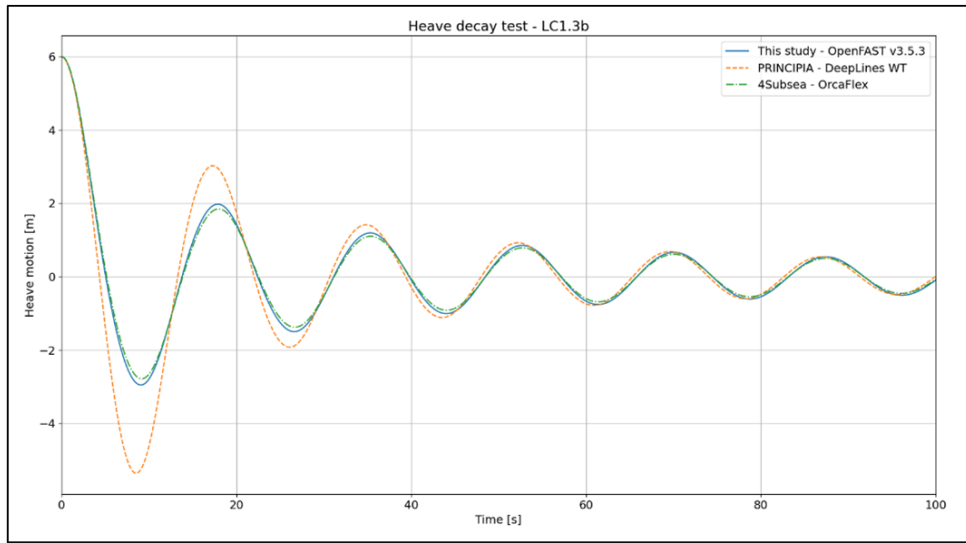


Figure 11: Heave motion on LC 1.3b heave decay test

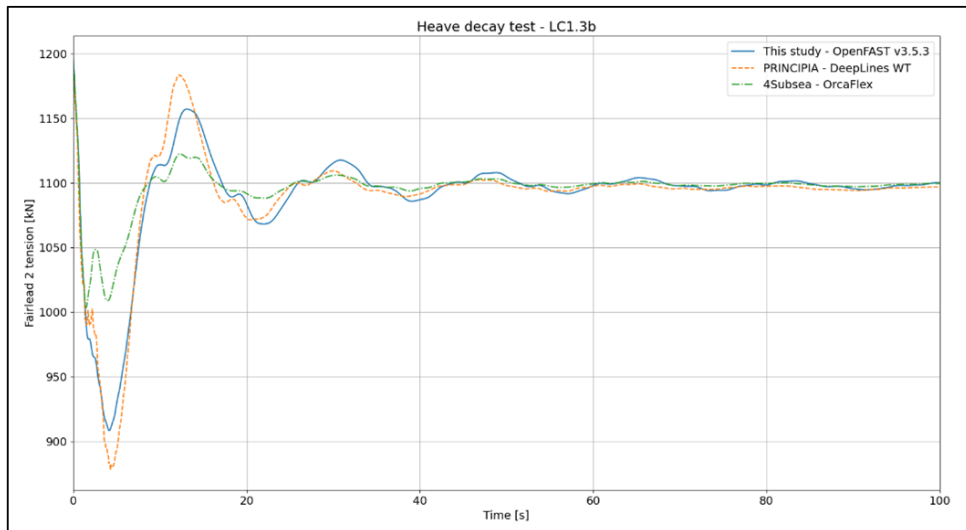


Figure 12: Fairlead tension on LC 1.3b heave decay test

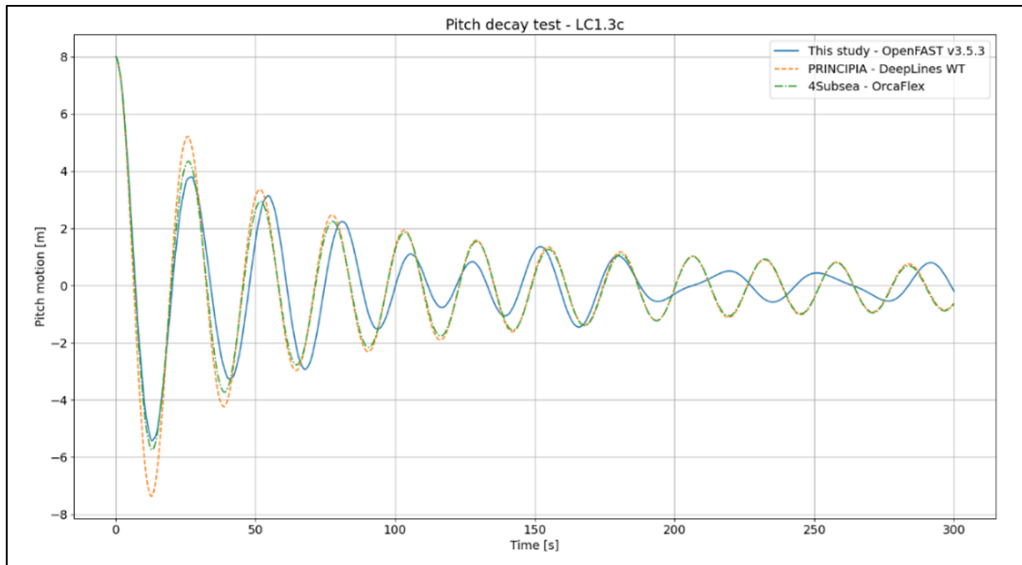


Figure 13: Pitch motion on LC 1.3c pitch decay test

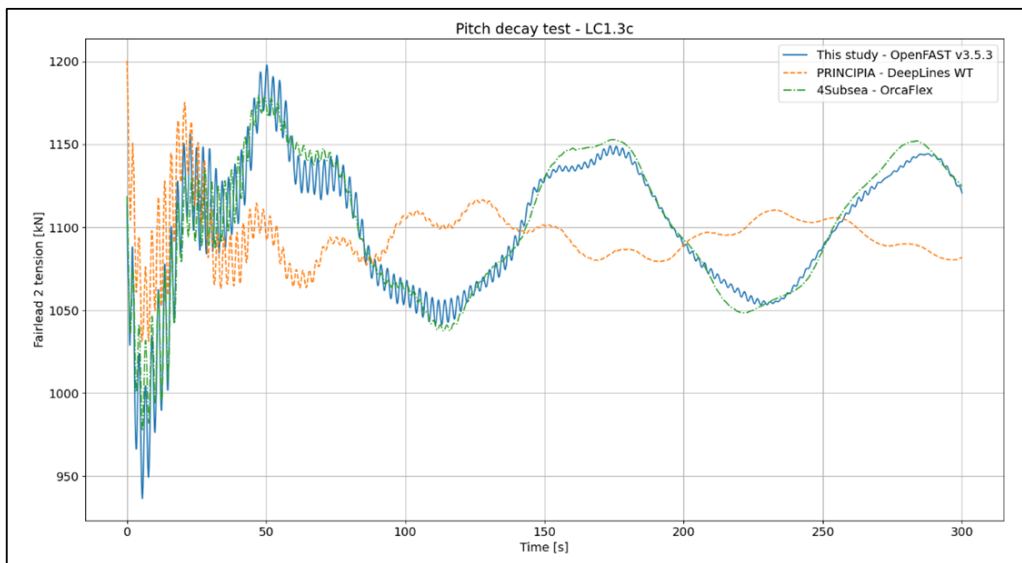


Figure 14: Fairlead tension on LC 1.3c pitch decay test

Table 2: Summary of the natural periods obtained from the decay tests

DOF	OpenFAST v3.5.3 (this study)	Physical model test (Coulling, Goupee, Robertson, Jonkman, & Dagher, 2013)
Surge	111.0 s	107.0 s
Heave	17.6 s	17.5 s
Pitch	25.0 s	26.8 s

## 2.2 Regular and irregular waves

In this Section, comparisons are made for the LC 2.1 and LC 2.2 shown in Table 1. No aerodynamic load is modeled and degrees of freedom correspond to the rotor, blade, generator and drive-train are switched off. Figure 15 shows the comparison of the motions for the regular wave case LC 2.1. All codes converged to the same amplitude and phase of the motions, with only slight deviation in the surge motion. This discrepancy in surge can be attributed to the inclusion of full Quadratic Transfer Function (QTF) in the results of this study. Consequently, the tension for LC 2.1 also demonstrated good agreement between the codes, shown in Figure 16. As for the irregular wave Load Case (LC) 2.2, the power spectral density of the motion response and tension are compared between this study and the results from DeepLines WT and Orcaflex, shown in Figure 17 and Figure 18. In the low frequencies region, the motion and tension in this study yields higher peaks than the reference results. These discrepancies in low frequencies are expected due to the contribution of the difference-frequency second order wave forces that is modeled in this study via full QTF. However, the peaks correspond to the first order wave frequencies are showing good agreement between all codes.

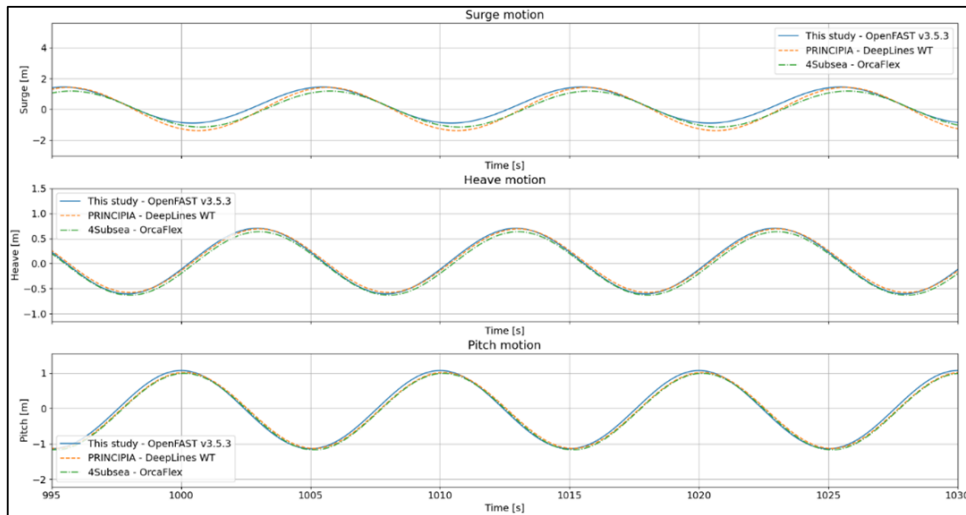


Figure 15: Motion response on LC 2.1 regular waves

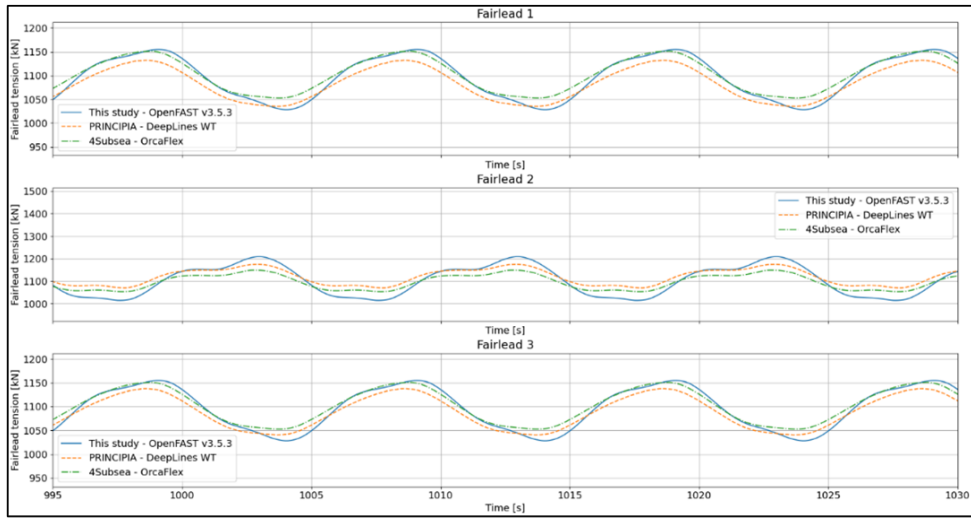


Figure 16: Fairlead tension on LC 2.1 regular waves

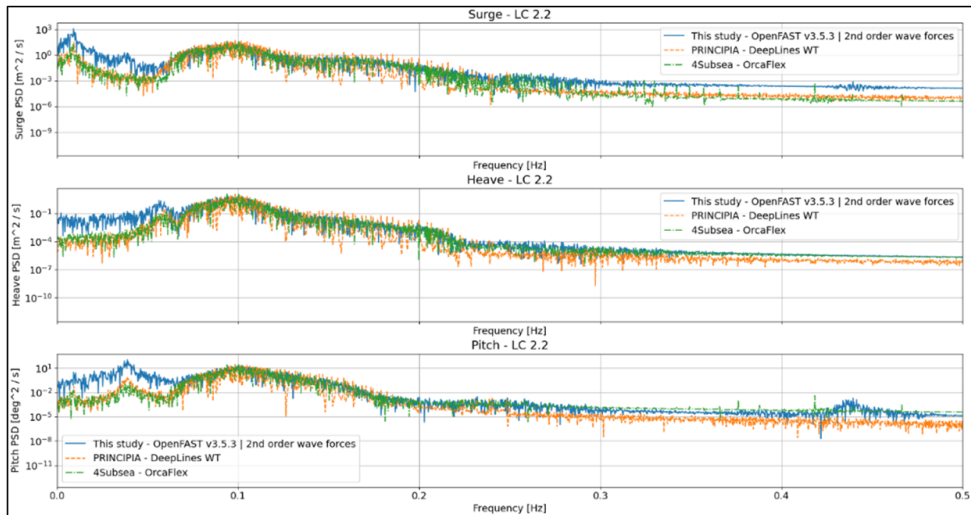


Figure 17: PSD motion response on LC 2.2 irregular waves

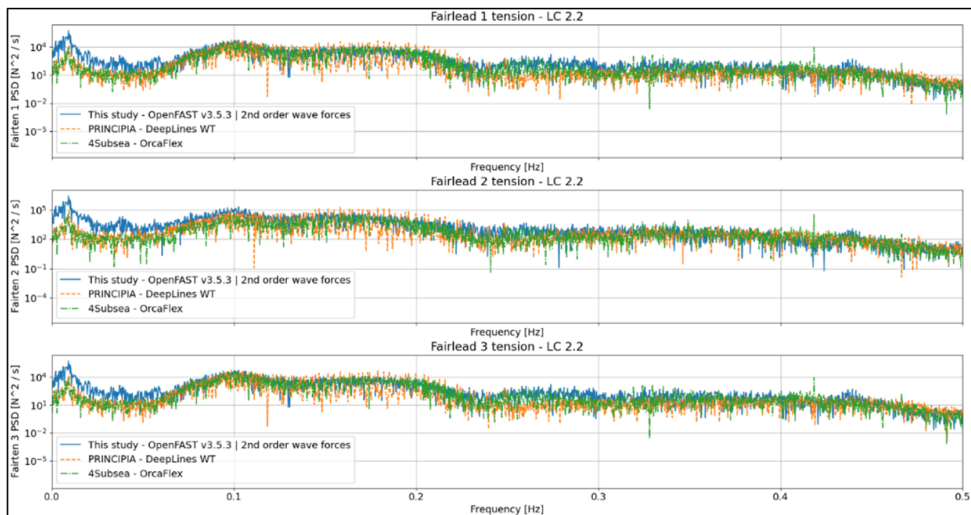


Figure 18: PSD fairlead tension on LC 2.2 irregular waves

### 2.3 Wind and waves combination

Lastly, a fully coupled system with the combination of aerodynamic and hydrodynamic forces are included. The simulation consists of 8.0 m/s wind speed aligned/parallel with the regular wave of 6.0 m and wave period of 10.0 s. This is below the rated wind speed of 11.4 m/s, hence, the rated power of 5000.0 kW is not achieved. This is shown in Figure 19 where the power generated from this study is below the reference results, albeit they have the same phase. In terms of motion response, all codes show an almost perfect agreement. Only the heave response has a minor deviation, which can be attributed to the modeling of heave disk which requires a fine-tune of the correct axial drag coefficient. This slight deviation in heave may have contributed to the minor difference in the fairlead tension, mainly in fairlead 2, shown in Figure 21.

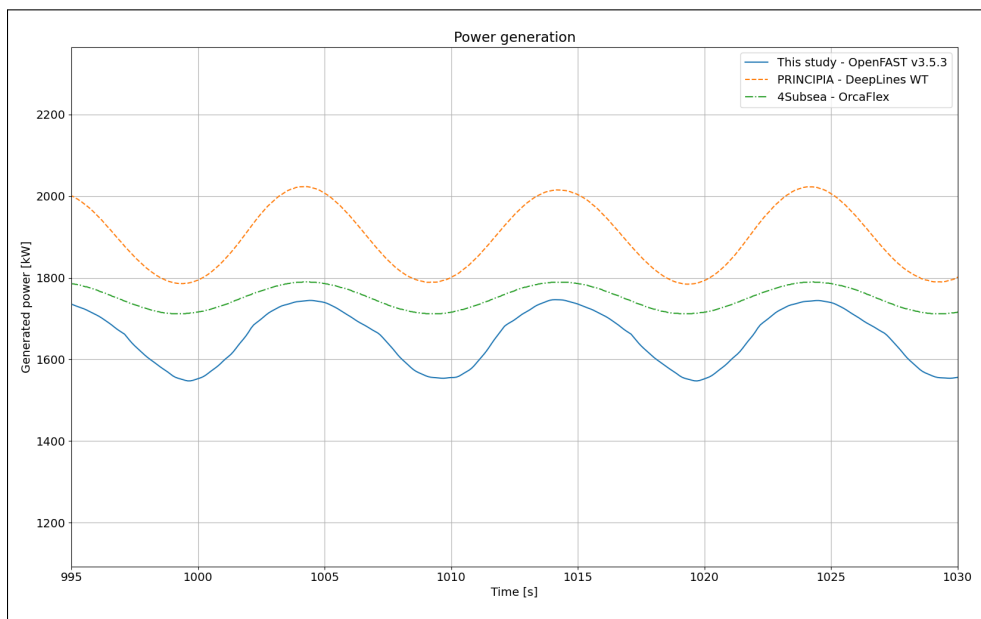


Figure 19: Generated power on LC3.1

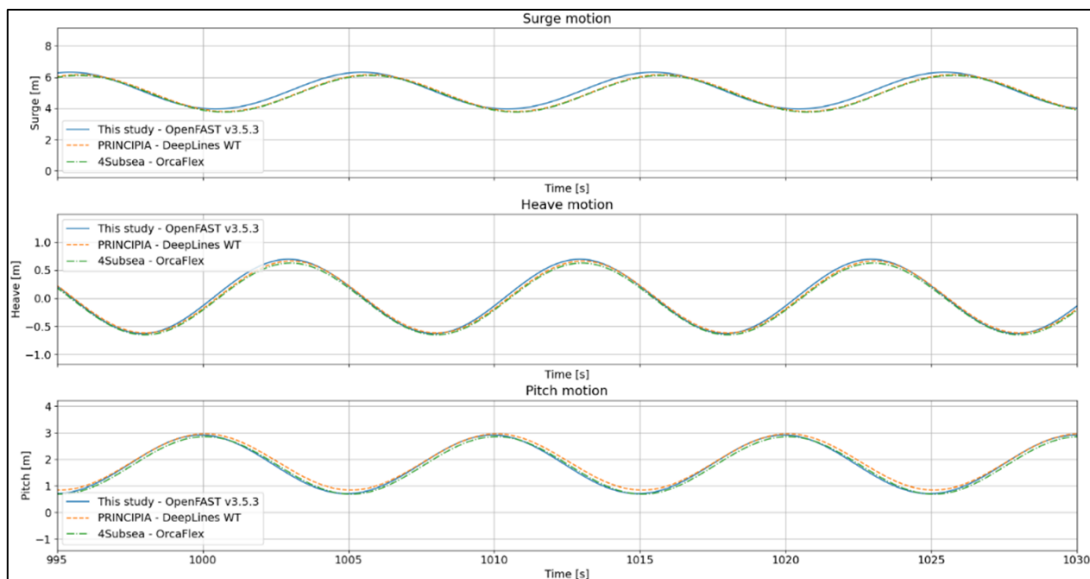


Figure 20: Motion response on LC 3.1

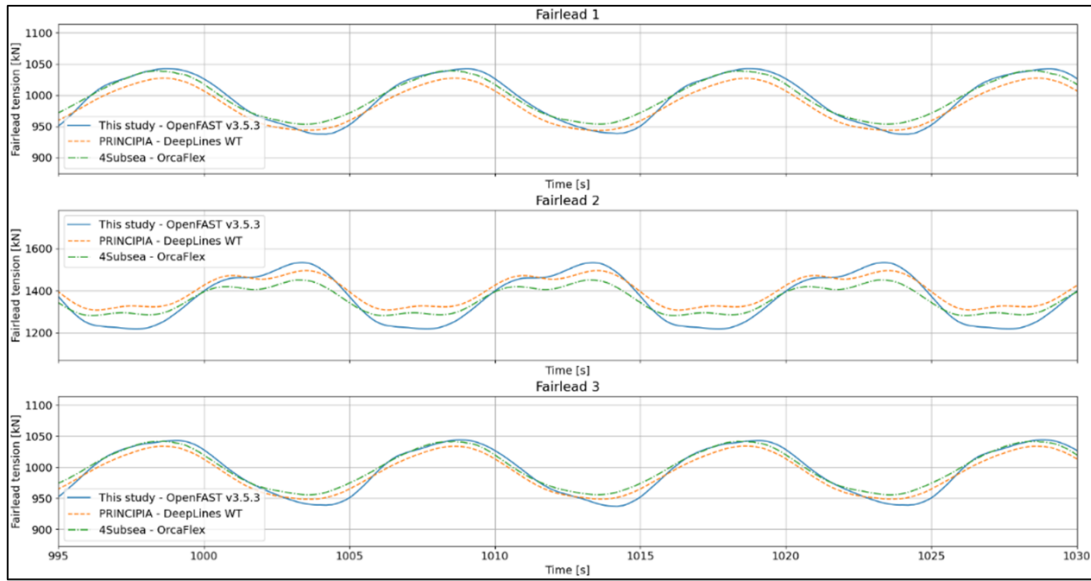


Figure 21: Fairlead tension on LC3.1

### 3 Simulation matrix

Presented in Table 3 are the different variables that are simulated for the irregular wave cases. All combinations of the variables are performed, resulting a total of 768 different irregular wave simulations. Note that JONSWAP spectrum with a peak enhancement factor of 3.3 is used. The choice of the wave conditions represents the range of Normal Sea State (NSS) to the Extreme Sea State (ESS). The wind speeds are chosen to cover the range of below and above the rated speed of 11.4 m/s. Wind and wave misalignment cases are performed with the nacelle always oriented perpendicular to the wind direction, as such that the optimum rated power is generated. Table 4 shows the combinations of variables in the regular wave simulation cases. All combinations are simulated resulting a total of 384 regular wave simulations. The simulation time for an irregular wave case is set to 1 hour. For a regular wave case, the simulation time is terminated after 10 minutes. The OpenFAST output file name contains the combination of variables in the following order: scenario, significant wave height/regular wave height, wave peak period/regular wave period, wind speed, wind direction, wind field. Table 5 shows the example of the output name for the combination shown in Table 6. The visualization of the example simulation in Table 6 can be found in the following video: <https://www.youtube.com/watch?v=KhqpHCLoVYY>.

Table 3: Simulation matrix in irregular wave cases

Scenario	Significant wave height	Wave peak period	Wind speed	Wind direction	Wind field
[-]	[m]	[s]	[m/s]	[deg]	[-]
Operational	1.5	8.0	8.0	0	Steady
Fairlead loss	3.0	10.0	11.0	30.0	Turbulent
	4.5	12.0	13.0	45.0	
	6.0	20.0	20.0		

Table 4: Simulation matrix in regular wave cases

Scenario	Regular wave height	Regular wave period	Wind speed	Wind direction	Wind field
[-]	[m]	[s]	[m/s]	[deg]	[-]
Operational	3.0	8.0	8.0	0	Steady
Fairlead loss	6.0	10.0	13.0	30.0	Turbulent
	9.0	12.0		45.0	
	12.0	20.0			

Table 5: Example of the output naming convention

Output name
[-]
operational_H12_T20_winspeed8_windir0_steady.out

Table 6: Example of the variables combination for the output in Table 5

Scenario	Regular wave height	Regular wave period	Wind speed	Wind direction	Wind field
[-]	[m]	[s]	[m/s]	[deg]	[-]
Operational	12.0	20.0	8.0	0	Steady

## 4 Selective results and discussion

In this Chapter, selective results are shown to assess the influence of the different variables that are simulated. Note that post-processing of the figures have been done using an open-source tool named [pyDatView](#) (Branlard, 2024). The software is able to load and visualize the output channels found in the OpenFAST output file (.out or .outb). Consequently, the labels for the x-axis and y-axis in the figures produced by [pyDatView](#) follow the ones written in the OpenFAST output channels.

### 4.1 Influence of second order wave forces

The HydroDyn module in OpenFAST supports different approaches to model the hydrodynamics of the sub-structure/platform. In this Section, the different hydrodynamic models are compared to assess their influence to the behaviour of the FOWT platform. Three different approaches are compared:

- Potential flow (PF)
- Potential flow with the inclusion of Morison drag
- Potential flow with the inclusion of Morison drag and full quadratic transfer function (QTF)

#### 4.1.1 Wave peak period of 8.0 s

This simulation compares the influence of full QTF and Morison drag for the wave peak period of 8.0 s. The load combination is summarized in Table 7. Figure 22 shows the time series of surge and heave motion. It can be observed that modeling full QTF induces slowly varying drift in the surge motion, on top of the first order motion, shown in orange dashed line. These responses in the lower frequency region can be seen in Figure 23 where the power spectral density (PSD) of the motion is shown. Additionally, modeling full QTF also results in larger heave amplitude. Figure 24 shows the responses during the transient state, at the beginning of the simulation. It can be concluded that modeling Morison drag dampened the surge and heave motion in the transient region. This is especially true for the heave motion where the effect of heave disk is modeled via the Morison drag in the axial direction. However, fine-tuning drag coefficients with experimental data is required to accurately predict the response due to the viscous effect. The difference in motion responses translate to the discrepancies observed in the fairlead tensions. As shown in Figure 25, the inclusion of full QTF induces large peaks in fairlead 2 tension. Furthermore, the tower base pitch moment is affected by the second order wave forces. As shown in Figure 26, peaks are observed in the lower and higher (than the first order wave) frequency regions. This can be attributed to the contribution of the difference- and sum-frequency second order wave forces, respectively.

Table 7: Load combination for the simulation in Subsection 4.1.1

Scenario	Significant wave height	Wave peak period	Wind speed	Wind direction	Wind field
[-]	[m]	[s]	[m/s]	[deg]	[-]
Operational	6.0	8.0	11.0	0	Steady

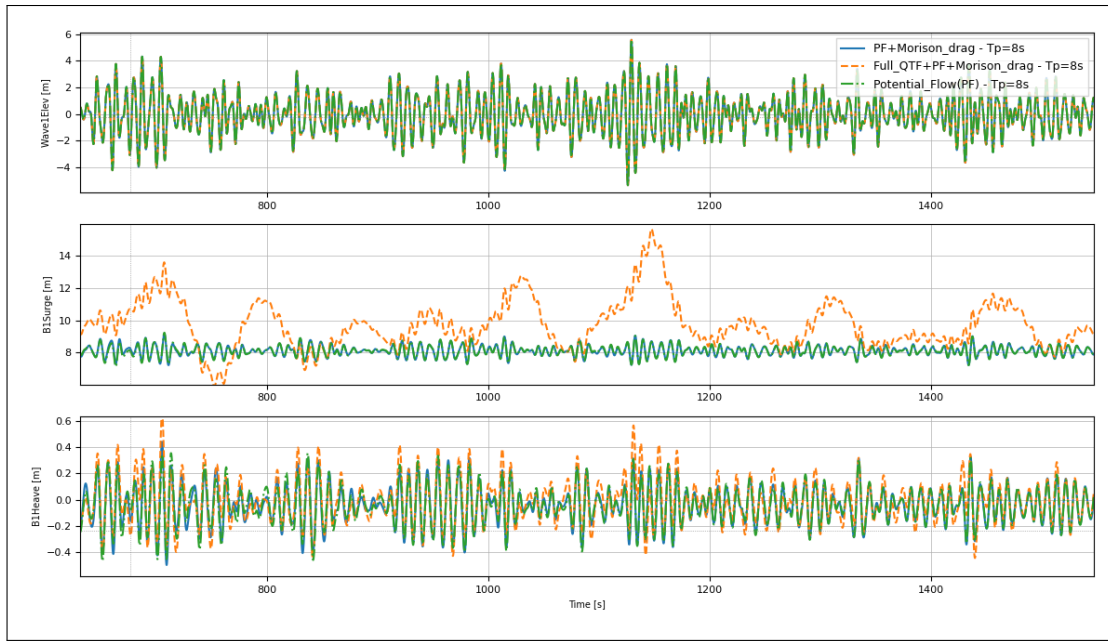


Figure 22: Time series of motion for the simulation in Subsection 4.1.1

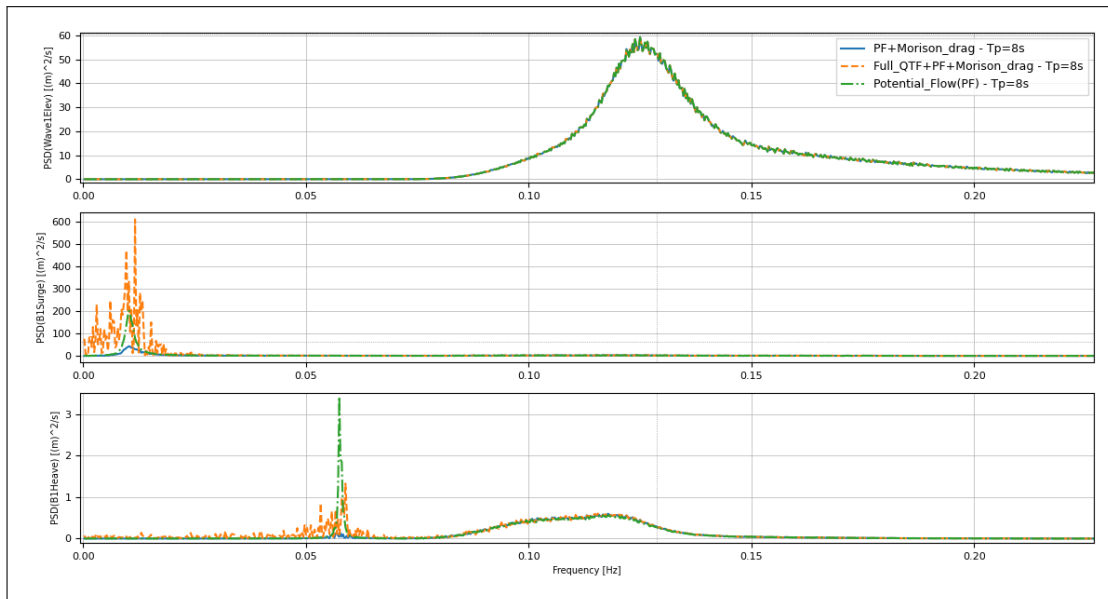


Figure 23: PSD of motion for the simulation in Subsection 4.1.1

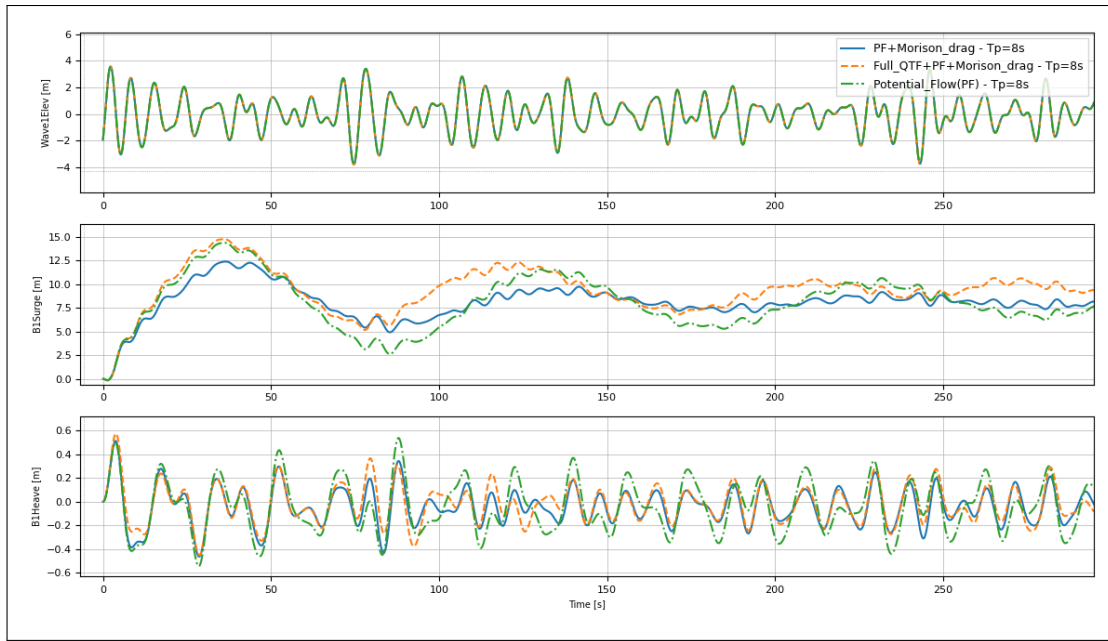


Figure 24: Time series of motion in the transient region for the simulation in Subsection 4.1.1

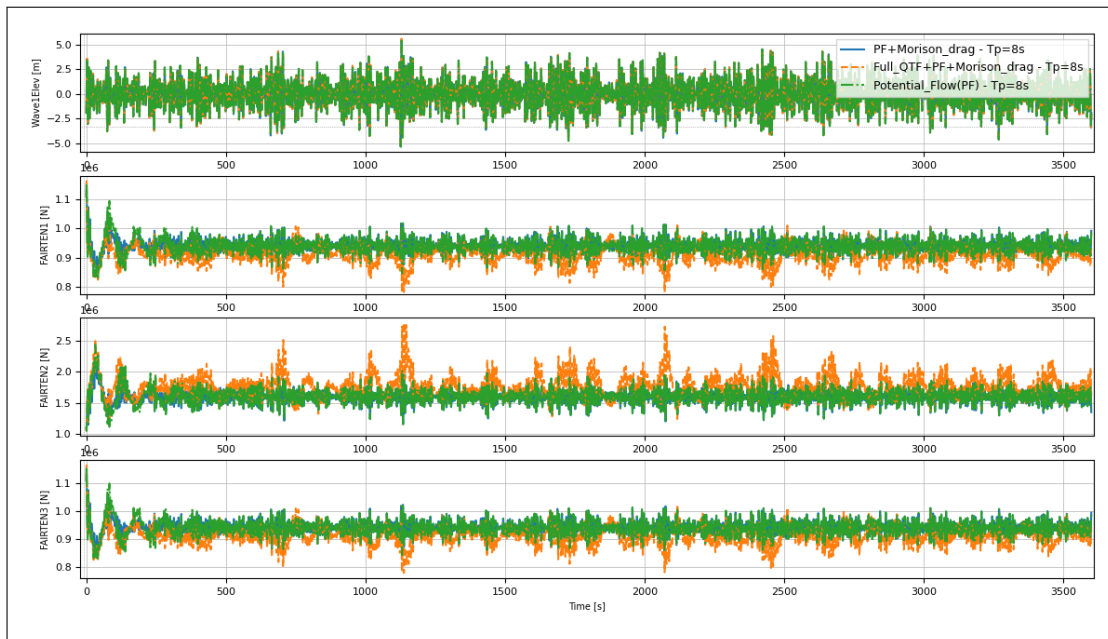


Figure 25: Time series of tension for the simulation in Subsection 4.1.1

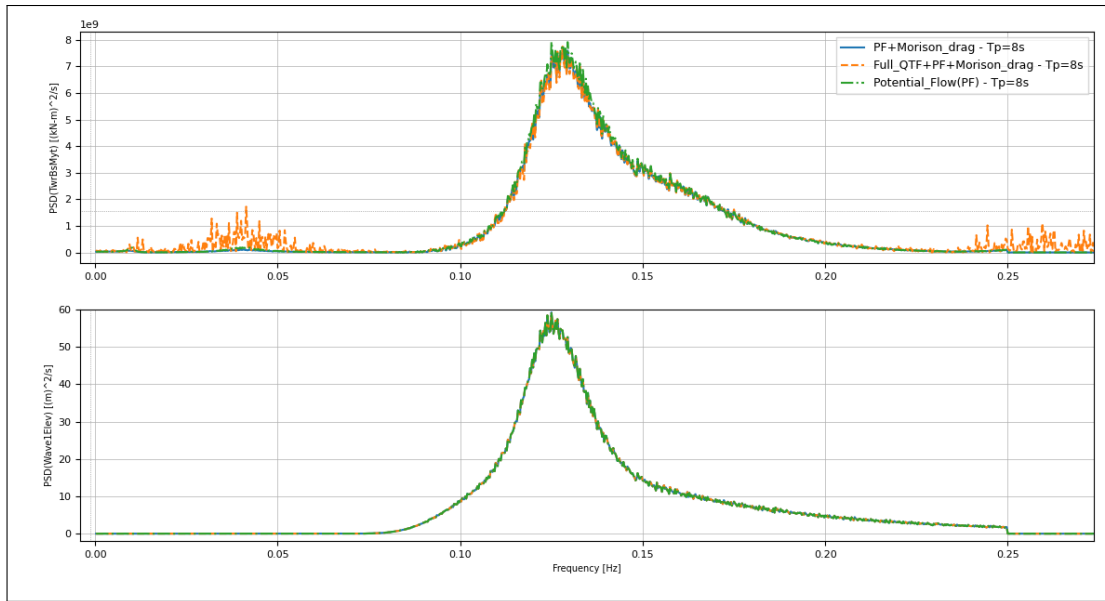


Figure 26: PSD of tower base pitch moment for the simulation in Subsection 4.1.1

#### 4.1.2 Wave peak period of 20.0 s

The influence of the different hydrodynamic models to the FOWT behaviour subjected to long waves is investigated in this simulation case. The load combination for this simulation is shown in Table 8. Figure 27 shows the motion responses in surge and heave. The surge motion has larger amplitudes when modeling the full QTF, albeit less apparent than the short waves simulation case in Subsection 4.1.1. The impact of second order wave forces to the responses in the lower frequency region can be seen when looking at the surge PSD, shown in Figure 28. On the other hand, heave motion shows identical responses for all modeling approaches. This can be observed when isolating the first 600.0 s of the simulation, namely the transient region, shown in Figure 29. In this case, the inclusion of Morison drag is less influential to the motion responses, compared to the short period waves simulation in Subsection 4.1.1. As for the fairlead tension, modeling full QTF results in a slightly higher fairlead tensions, shown in Figure 30. This is also true when comparing the tower base pitch moment. Results with the inclusion of full QTF has slightly larger pitch moment, as shown in Figure 31. It can be concluded that for the wave peak period of 20.0 s, including the Morison drag and full QTF is less influential compared to the simulation with the wave peak period of 8.0 s in Subsection 4.1.1.

Table 8: Load combination for the simulation in Subsection 4.1.2

Scenario	Significant wave height	Wave peak period	Wind speed	Wind direction	Wind field
[-]	[m]	[s]	[m/s]	[deg]	[-]
Operational	6.0	20.0	11.0	0	Steady

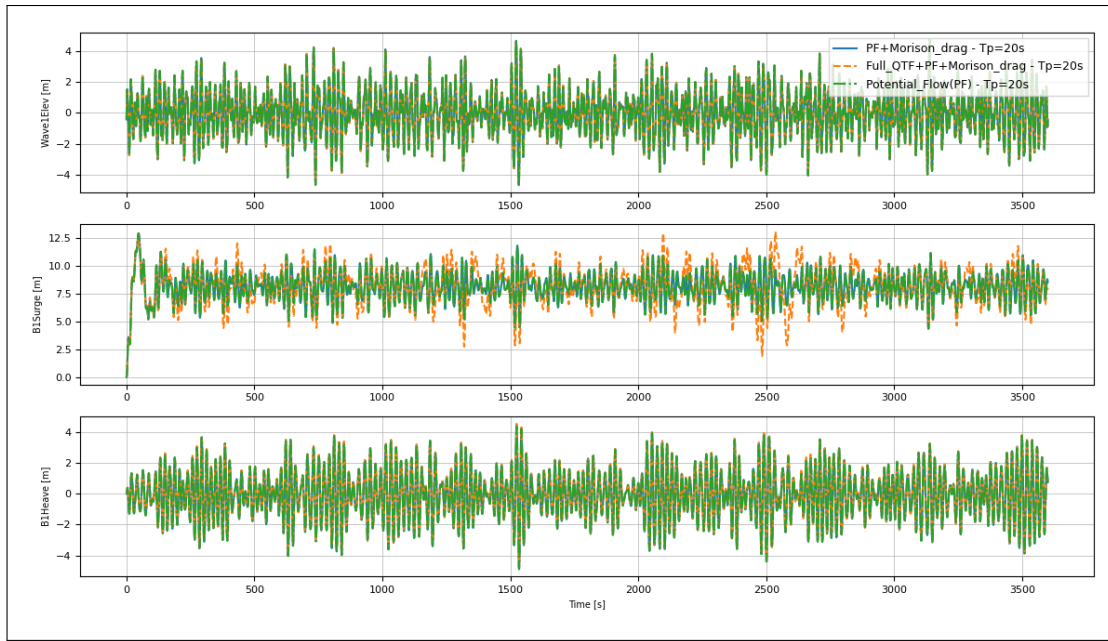


Figure 27: Time series of motion for the simulation in Subsection 4.1.2

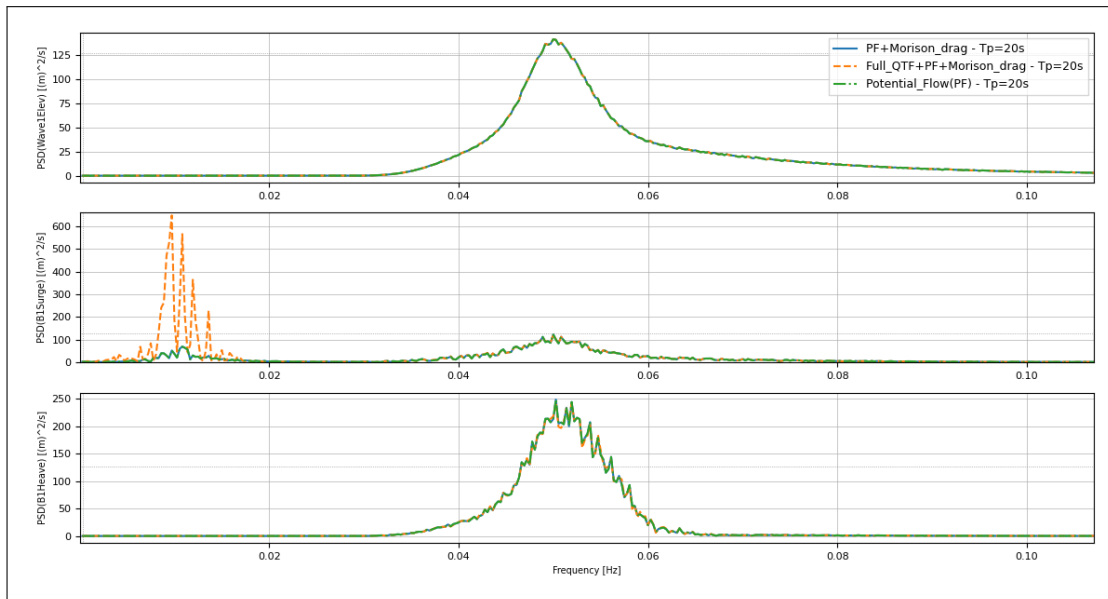


Figure 28: PSD of motion for the simulation in Subsection 4.1.2

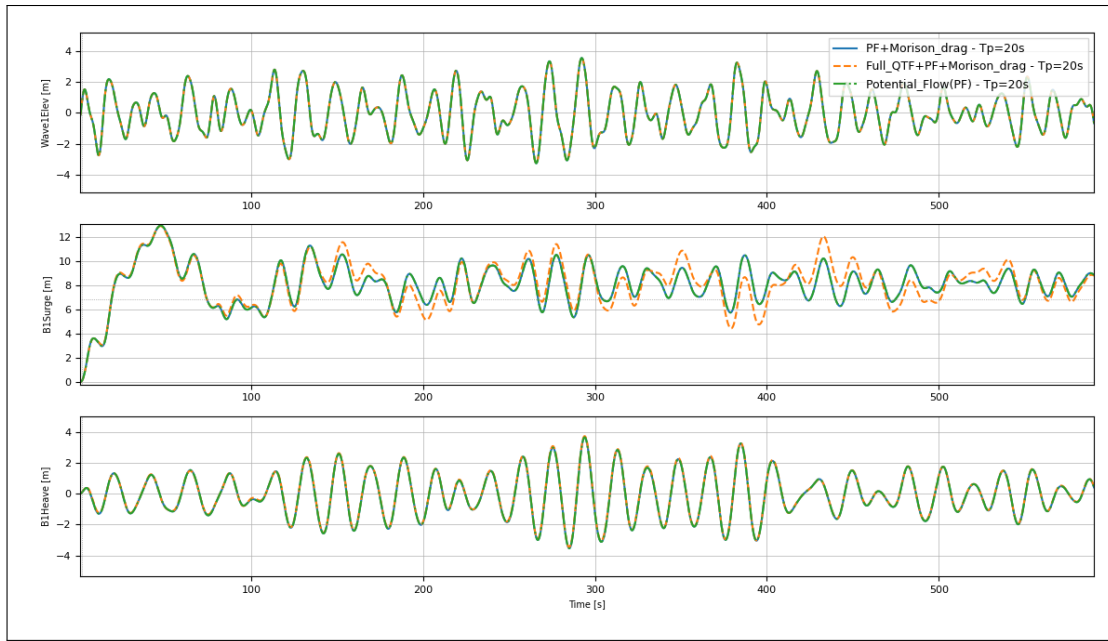


Figure 29: Time series of motion in the transient region for the simulation in Subsection 4.1.2

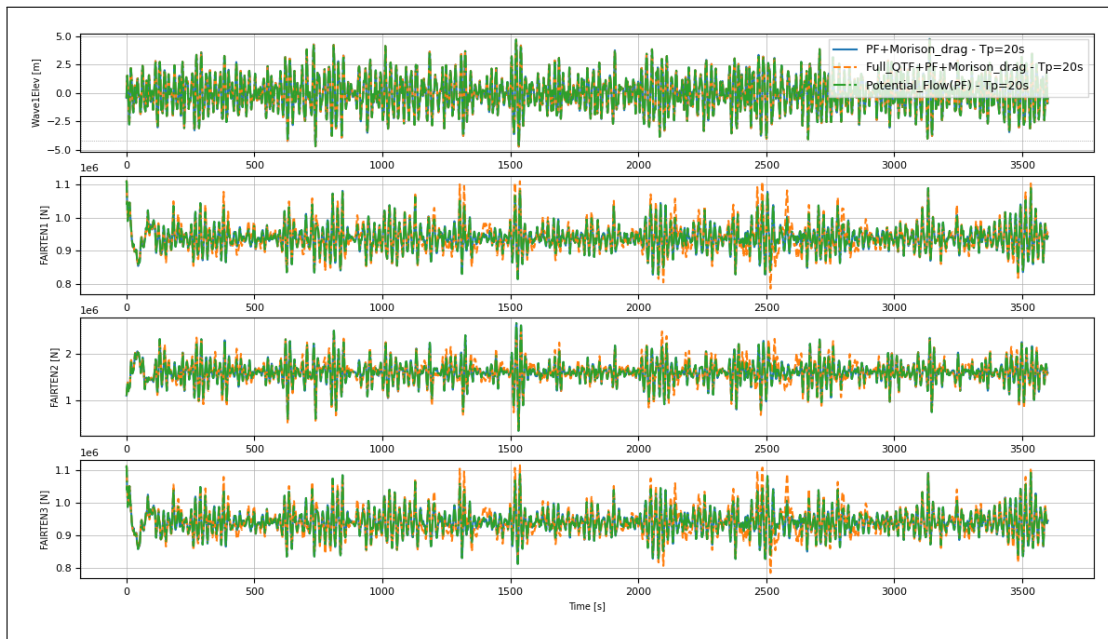


Figure 30: Time series of tension for the simulation in Subsection 4.1.2

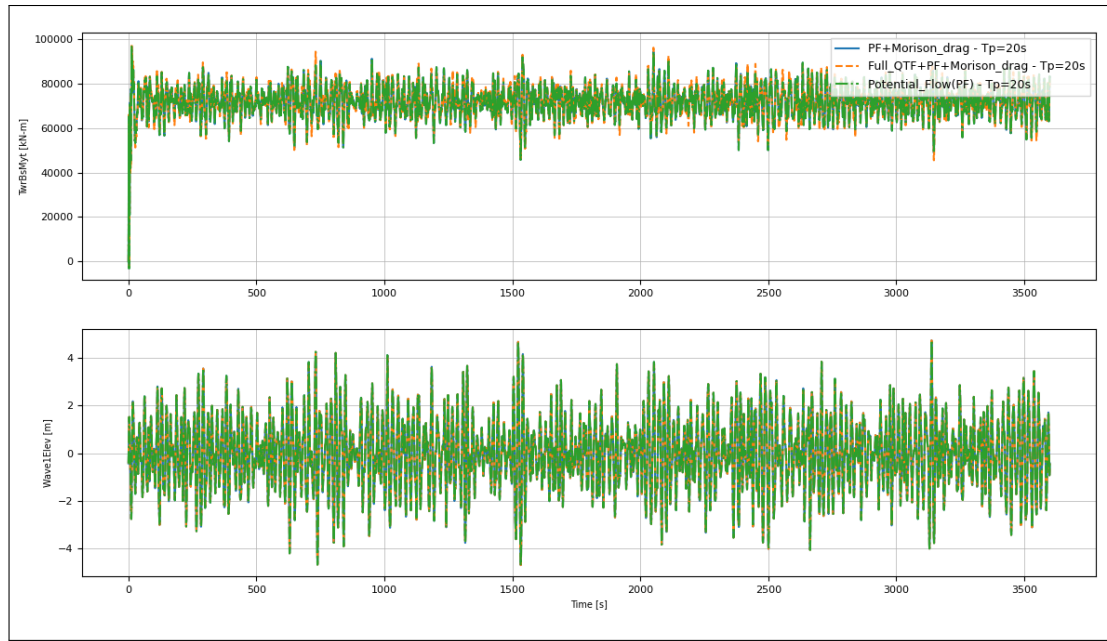


Figure 31: Time series of tower base pitch moment for the simulation in Subsection 4.1.2

## 4.2 Influence of wave period

In this Section, a comparison between the different regular wave periods for the same regular wave height of 12.0 m is presented. Note that the hybrid approach (potential flow combined with Morison drag) with the inclusion of full QTF is used to model the hydrodynamics interaction of the platform. Summarized in Table 9 are the load combinations simulated in this comparison. Figure 32 shows the comparison of surge, heave and pitch responses of the platform subjected to wave periods of 8.0, 10.0, 12.0 and 20.0 seconds, respectively. In surge, the contribution of mean-drift from the difference-frequency second order wave forces is most apparent when the platform is subjected to the wave period of 8.0 s. A significantly larger heave amplitude is observed when the platform is encountering a regular wave period of 20.0 s. This is due to the fact that the regular wave period of 20.0 s is close to the natural period of the platform, which is 17.6 s, shown in Table 2. In a similar way, pitch motion due to the wave period of 20.0 s has the largest response amplitude, as the pitch natural period of the platform is 25.0 s. The large heave and pitch motion amplitudes experienced by the platform when it is subjected to the wave period of 20.0 s are translated to the fairlead 1 and 3, which results in the largest tension amplitudes. Mean-drift has a significant influence to the fairlead 2 (mooring line that is parallel to the wave propagation), as shown in Figure 33, the simulation against wave period of 8.0 s results in the largest peak tension. Shown in Figure 34 is the time series of the tower base pitch moment. The simulation with a regular wave period of 8.0 s (shortest wave in the comparison) results in a significantly larger tower base pitch moment compared to all other wave periods. When observing the PSD, a significant peak at 0.25 Hz, which is two times the wave frequency of 0.125 Hz (wave period of 8.0 s) is present. This is due to influence of the sum-frequency second order wave forces. The impact is less apparent on other frequencies except for the frequency of 0.10 Hz (wave period of 10.0 s) where the peak at 0.20 Hz is observed. From this comparison, it can be concluded that the wave period of 8.0 s results in the highest fairlead 2 tension and the largest tower base pitch amplitude

moment.

Table 9: Load combination for the simulation in Section 4.2

Scenario	Regular wave height	Regular wave period	Wind speed	Wind direction	Wind field
[-]	[m]	[s]	[m/s]	[deg]	[-]
Operational	12.0	8.0, 10.0, 12.0, 20.0	13.0	0	Steady

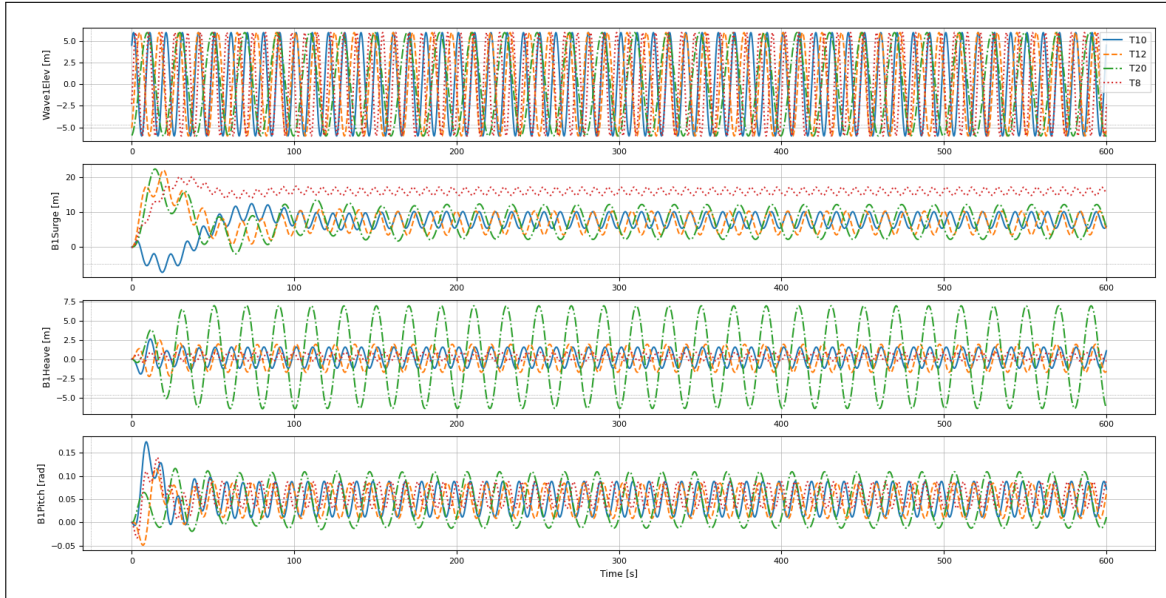


Figure 32: Time series of motion for the simulation in Section 4.2

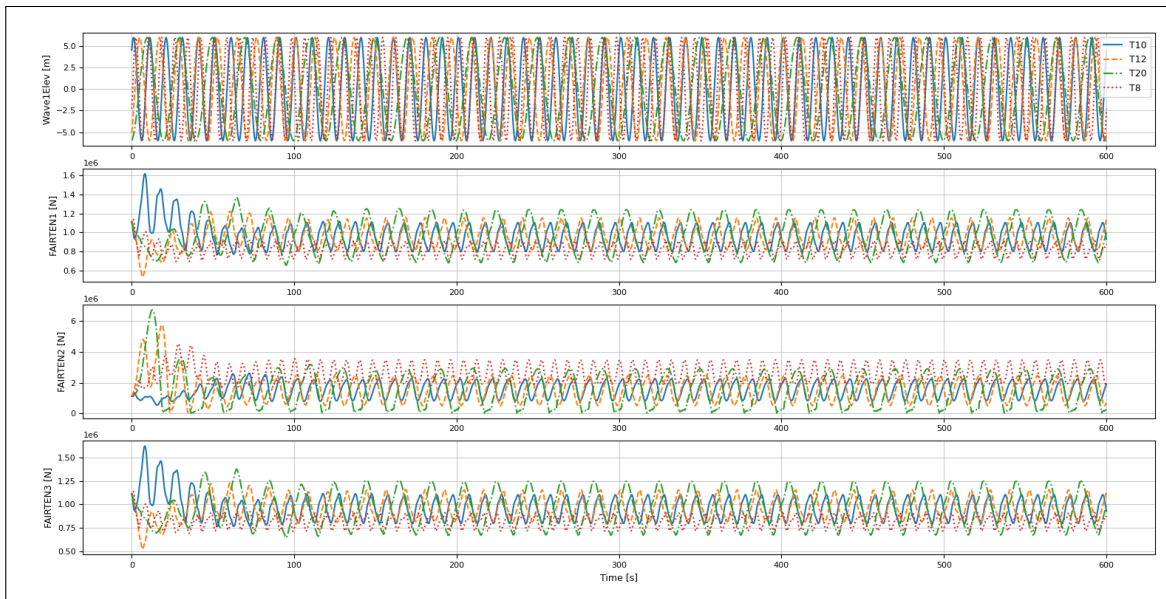


Figure 33: Time series of tension for the simulation in Section 4.2

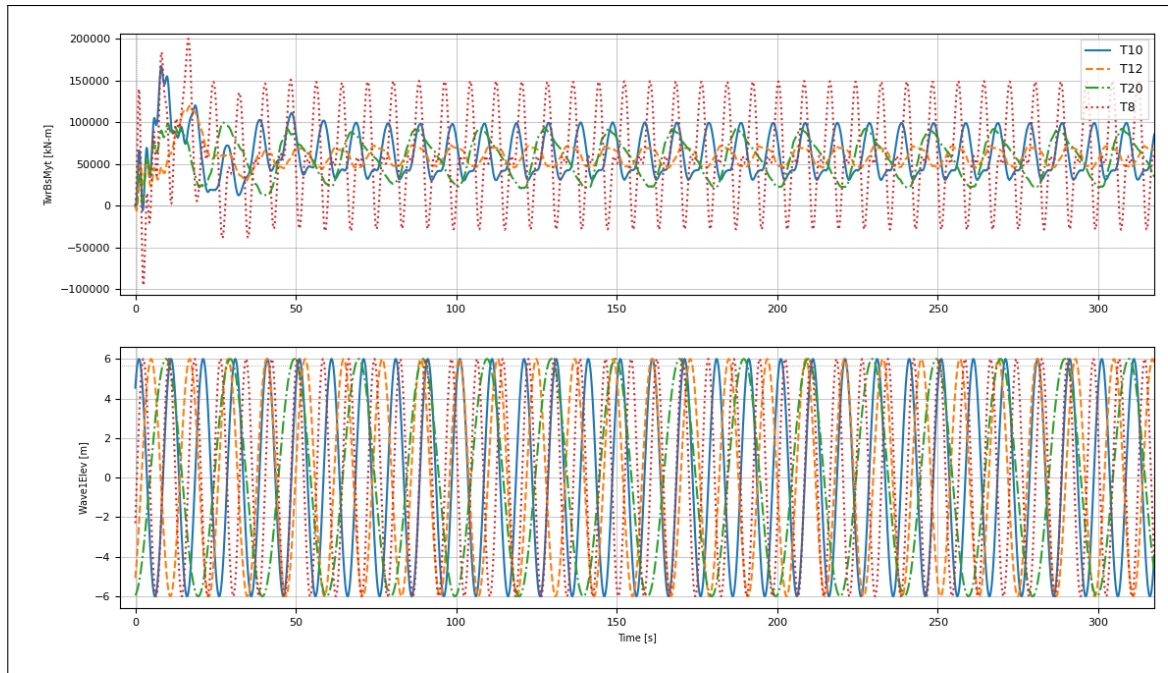


Figure 34: Time series of tower base pitch moment for the simulation in Section 4.2

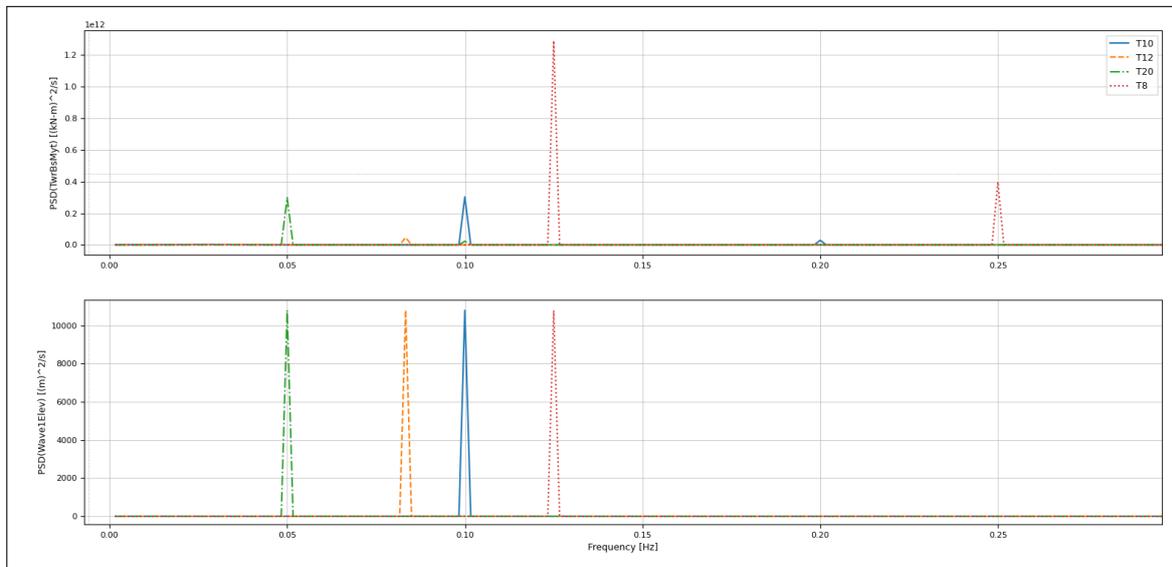


Figure 35: PSD of tower base pitch moment for the simulation in Section 4.2

### 4.3 Damaged scenario

The impact of losing one mooring line is assessed in this comparison. Table 10 listed the combination of input variables used in this comparison. The mooring fairlead 2 that is parallel to the wave propagation direction (see Figure 8) is detached/set free during the simulation. As shown in Figure 36, the platform drifted up to 800.0 m (solid blue line) compared to the simulation with intact mooring lines (orange dashed line). Furthermore, the loss of a mooring line caused the platform to pitch up to two folds more compared to the operational scenario. This is due to the thrust generated by the wind turbine to which in the operational scenario the load would have been transferred to the mooring

line at fairlead 2. This has an implication to the decrease in draft which can be seen in the heave response shown in Figure 36. Furthermore, this is also affecting the tower base moment. As shown in Figure 37, the damaged scenario results in higher maximum and minimum pitch moments due to the increase in the mean value. Additionally, for the remaining mooring lines, the damaged scenario introduced a slowly varying tension amplitudes (i.e., low frequency loads), on top of the tension due to the first order wave, shown in Figure 38.

Table 10: Load combination for the simulation in Section 4.3

Scenario	Significant wave height	Wave peak period	Wind speed	Wind direction	Wind field
[-]	[m]	[s]	[m/s]	[deg]	[-]
Operational, Fairlead 2 loss	6.0	8.0	13.0	0	Steady

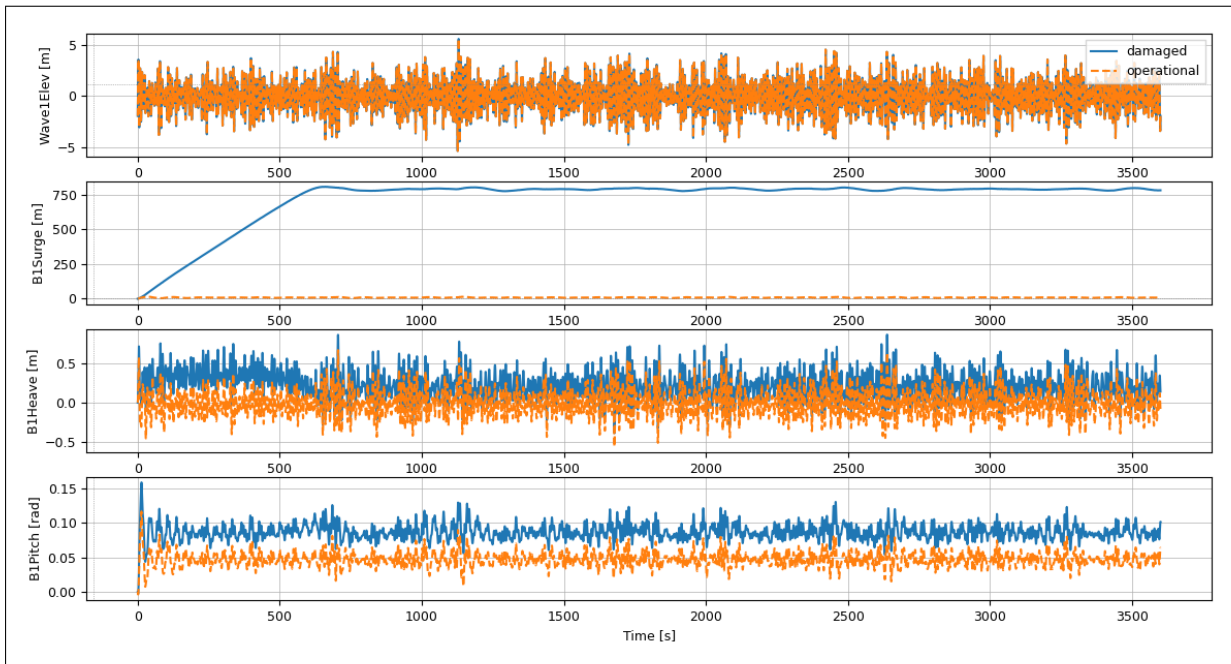


Figure 36: Time series of motion for the simulation in Section 4.3

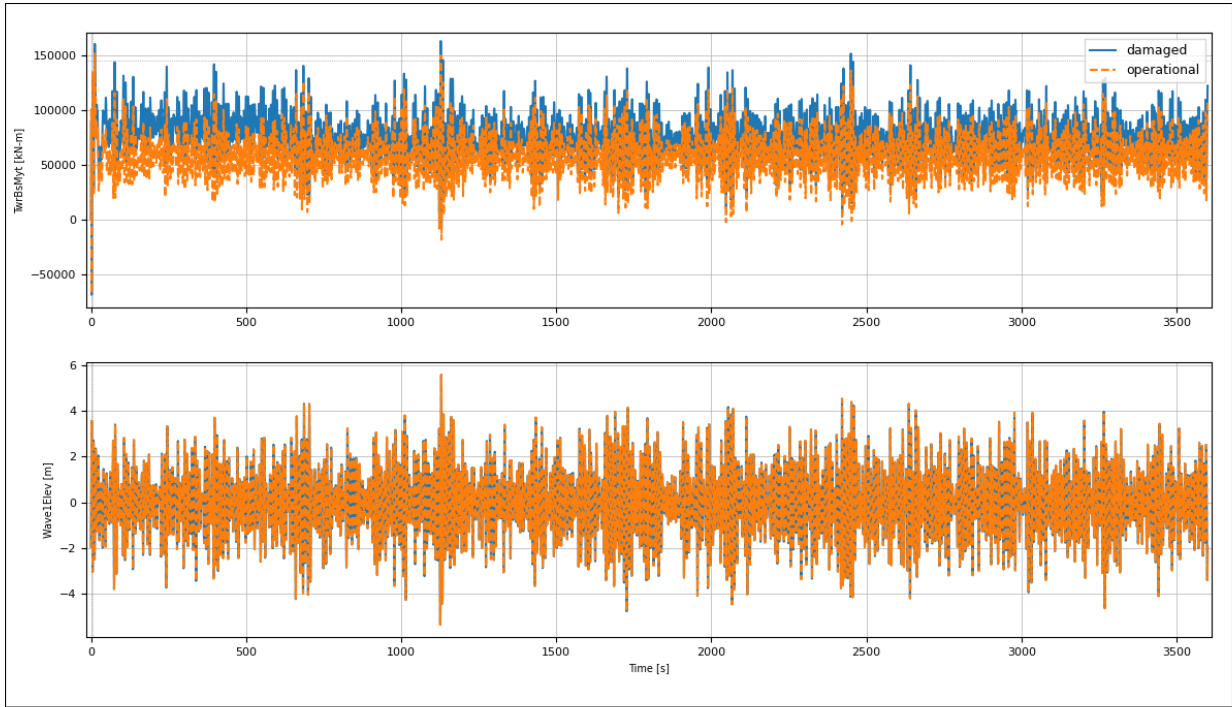


Figure 37: Time series of tower base pitch moment for the simulation in Section 4.3

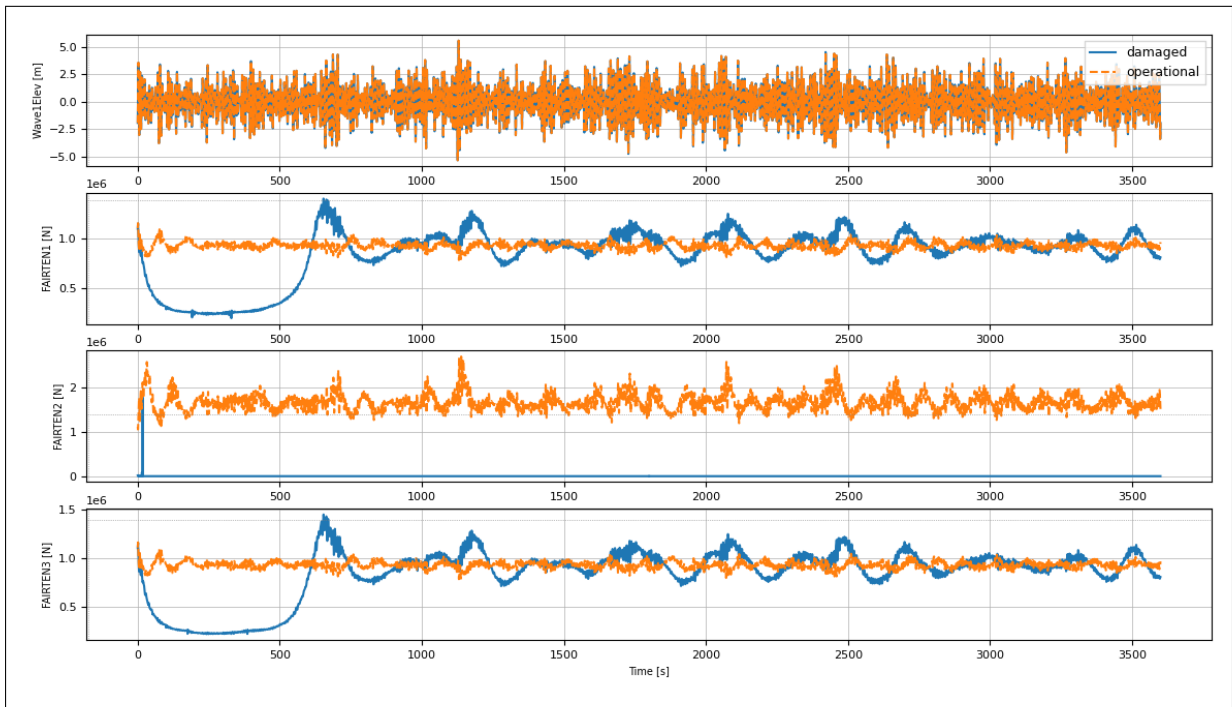


Figure 38: Time series of tension for the simulation in Section 4.3

## 5 Concluding remarks

As a deliverable in the BEL-Float project (D1.1.1.1), 1152 numerical simulations have been performed for the DeepCwind OC4 semi-submersible FOWT under various wind and waves conditions. A verification study was conducted against the numerical benchmark results found in (A. Robertson, Jonkman, Vorpahl, et al., 2014) and a physical experiment in (Coulling et al., 2013). The decay tests in this study matched well with the physical model test results. The numerical simulations against various load cases also agreed well with the benchmark study. A sensitivity study has been conducted to assess the influence of the different hydrodynamic modeling. Generally the inclusion of full QTF and Morison drag results in a more realistic behaviour, albeit fine-tuning of coefficients is required. A total of 783 OpenFAST output channels have been generated for each simulation. The global analysis time-domain numerical simulation results are distributed to the followings.

- Input for research Topic 3 in the [BEL-Float project](#): "Development of sensor topologies and operational modal analysis algorithms to assess and monitor the low frequency dynamics of floating offshore wind platform(s)."
- Input for research Topic 5 in the [BEL-Float project](#): "Development of numerical tools for fatigue damage assessment and lifetime prediction for a floating offshore wind platform subjected to multiple non-linear stochastic load sources". A report of Deliverable 1 from Topic 5 entitled "Multi-dimensional modelling strategy" has been published and can be found in (Rappe, 2024).
- Input for research Topic 6 in the [BEL-Float project](#): "Assessing dynamic power cable deformation, stresses and integrity using numerical modelling and operational modal analysis of DAS data"

Additionally, the dataset has been uploaded to the Zenodo open-access platform and is divided into the following sub-datasets:

- Part 1: (<https://doi.org/10.5281/zenodo.13927766>)
- Part 2: (<https://doi.org/10.5281/zenodo.13929486>)
- Part 3: (<https://doi.org/10.5281/zenodo.13933651>)
- Part 4: (<https://doi.org/10.5281/zenodo.13934602>)
- Part 5: (<https://doi.org/10.5281/zenodo.13935069>)
- Part 6: (<https://doi.org/10.5281/zenodo.13935243>)
- Part 7: (<https://doi.org/10.5281/zenodo.13939435>)
- Part 8: (<https://doi.org/10.5281/zenodo.13939715>)
- Part 9: (<https://doi.org/10.5281/zenodo.13940172>)
- Parent input files: (<https://doi.org/10.5281/zenodo.13940284>)

The load combinations for the corresponding sub-datasets can be found in Table 11 and Table 12.

Table 11: Load combinations for the sub-dataset Part 1 to 8

Dataset	Scenario	Significant wave height	Wave peak period	Wind speed	Wind direction	Wind field
[-]	[-]	[m]	[s]	[m/s]	[deg]	[-]
Part 1	Operational	6.0	8.0	8.0	0	Steady
			10.0	11.0	30.0	Turbulent
			12.0	13.0	45.0	
			20.0	20.0		
Part 2	Operational	4.5	8.0	8.0	0	Steady
			10.0	11.0	30.0	Turbulent
			12.0	13.0	45.0	
			20.0	20.0		
Part 3	Operational	3.0	8.0	8.0	0	Steady
			10.0	11.0	30.0	Turbulent
			12.0	13.0	45.0	
			20.0	20.0		
Part 4	Operational	1.5	8.0	8.0	0	Steady
			10.0	11.0	30.0	Turbulent
			12.0	13.0	45.0	
			20.0	20.0		
Part 5	damaged	6.0	8.0	8.0	0	Steady
			10.0	11.0	30.0	Turbulent
			12.0	13.0	45.0	
			20.0	20.0		
Part 6	damaged	4.5	8.0	8.0	0	Steady
			10.0	11.0	30.0	Turbulent
			12.0	13.0	45.0	
			20.0	20.0		
Part 7	damaged	3.0	8.0	8.0	0	Steady
			10.0	11.0	30.0	Turbulent
			12.0	13.0	45.0	
			20.0	20.0		
Part 8	Operational	1.5	8.0	8.0	0	Steady
			10.0	11.0	30.0	Turbulent
			12.0	13.0	45.0	
			20.0	20.0		

Table 12: Load combinations for the sub-dataset Part 9

Dataset	Scenario	Regular wave height	Regular wave period	Wind speed	Wind direction	Wind field	
[-]	[-]	[m]	[s]	[m/s]	[deg]	[-]	
Part 9	Operational	3.0	8.0	8.0	0	Steady	
	Fairlead loss	6.0	10.0	13.0	30.0	Turbulent	
		9.0	12.0				45.0
		12.0	20.0				

## References

- Bayati, I., Jonkman, J., Robertson, A., & Platt, A. (2014, 7). Effects of second-order hydrodynamics on a semisubmersible floating offshore wind turbine: Preprint. , 524. Retrieved from <https://www.osti.gov/biblio/1144826> doi: 10.1088/1742-6596/524/1/012094
- Branlard, E. (2024). *pydatview*. Retrieved from <https://github.com/ebanlard/pyDatView>
- Coulling, A. J., Goupee, A. J., Robertson, A. N., Jonkman, J. M., & Dagher, H. J. (2013, 03). Validation of a FAST semi-submersible floating wind turbine numerical model with DeepCwind test data. *Journal of Renewable and Sustainable Energy*, 5(2), 023116. Retrieved from <https://doi.org/10.1063/1.4796197> doi: 10.1063/1.4796197
- Cummins, W. (1962). The Impulse Response Function and Ship Motions. *Schiffstechnik*, 9, 101–109.
- Goupee, A. J., Fowler, M. J., Kimball, R. W., Helder, J., & de Ridder, E.-J. (2014, 06). *Additional wind/wave basin testing of the deepcwind semi-submersible with a performance-matched wind turbine* (Vol. Volume 9B: Ocean Renewable Energy). Retrieved from <https://doi.org/10.1115/OMAE2014-24172> doi: 10.1115/OMAE2014-24172
- Goupee, A. J., Koo, B., Lambrakos, K., & Kimball, R. (2012, 04). *Model tests for three floating wind turbine concepts*. Retrieved from <https://doi.org/10.4043/23470-MS> doi: 10.4043/23470-MS
- Hall, M. (2020, 12). Moordyn v2 new capabilities in mooring system components and load cases. Retrieved from <https://www.osti.gov/biblio/1766856> doi: 10.1115/OMAE2020-19341
- Hall, M., & Goupee, A. (2015). Validation of a lumped-mass mooring line model with deepcwind semisubmersible model test data. *Ocean Engineering*, 104, 590-603. Retrieved from <https://www.sciencedirect.com/science/article/pii/S0029801815002279> doi: <https://doi.org/10.1016/j.oceaneng.2015.05.035>
- International Energy Agency. (2024). *Iea task 30*. Retrieved from <https://iea-wind.org/task30/>
- Jonkman, B., Platt, A., Mudafort, R. M., Branlard, E., Sprague, M., Ross, H., ... Carmo, L. (2024, April). Openfast/openfast: v3.5.3. Retrieved from <https://doi.org/10.5281/zenodo.10962897> doi: 10.5281/zenodo.10962897
- Jonkman, B. J. (2014, 10). Turbsim user's guide v2.00.00. Retrieved from [https://www.nrel.gov/wind/nwtc/assets/downloads/TurbSim/TurbSim\\_v2.00.pdf](https://www.nrel.gov/wind/nwtc/assets/downloads/TurbSim/TurbSim_v2.00.pdf)
- Jonkman, J., Branlard, E., Hall, M., Hayman, G., Platt, A., & Robertson, A. (2020). Implementation of substructure flexibility and member-level load capabilities for floating offshore wind turbines in openfast. Retrieved from <https://www.osti.gov/biblio/1665796> doi: 10.2172/1665796
- Jonkman, J. M. (2005). Fast coordinate systems. *National Renewable Energy Laboratory*. Retrieved from [https://openfast.readthedocs.io/en/dev/\\_downloads/c9ae932057ea1e64c79154b36d3ab30a/FASTCoordinateSystems.doc](https://openfast.readthedocs.io/en/dev/_downloads/c9ae932057ea1e64c79154b36d3ab30a/FASTCoordinateSystems.doc)
- Jonkman, J. M., & Buhl, M. L., Jr. (2005). Fast user's guide - updated august 2005. *National Renewable Energy Laboratory*. Retrieved from

- <https://www.osti.gov/biblio/15020796> doi: 10.2172/15020796
- Jonkman, J. M., Robertson, A., & Hayman, G. J. (2014). Hydrodyn user's guide and theory manual. *National Renewable Energy Laboratory*. Retrieved from [https://www.nrel.gov/wind/nwtc/assets/downloads/HydroDyn/HydroDyn\\_Manual.pdf](https://www.nrel.gov/wind/nwtc/assets/downloads/HydroDyn/HydroDyn_Manual.pdf)
- Morison, J. R., O'Brien, M. P., Johnson, J. W., & Schaaf, S. (1950). The force exerted by surface wave on piles. *Transactions of the American Institute of Mining & Metallurgical Engineers*, 189, 147–164.
- OpenFAST. (2024a). *Openfast module documentation*. Retrieved from <https://openfast.readthedocs.io/en/main/source/user/index.html#module-documentation>
- OpenFAST. (2024b). *r-test*. [https://github.com/OpenFAST/r-test/tree/main/glue-codes/openfast/5MW\\_OC4Semi\\_WSt\\_WavesWN](https://github.com/OpenFAST/r-test/tree/main/glue-codes/openfast/5MW_OC4Semi_WSt_WavesWN). GitHub. (commit 548bf2143633a7066f4582167fdf4180951fd7f6)
- OWI-lab. (2024). *Bel-float*. Retrieved from <https://www.owi-lab.be/bel-float>
- Platt, A., Jonkman, B., & Jonkman, J. M. (2016). Inflowwind user's guide. *National Renewable Energy Laboratory*. Retrieved from [https://www.nrel.gov/wind/nwtc/assets/downloads/InflowWind/InflowWind\\_Manual.pdf](https://www.nrel.gov/wind/nwtc/assets/downloads/InflowWind/InflowWind_Manual.pdf)
- Pribadi, A., Donatini, L., Lataire, E., Fernandez, G. V., & Martínez-Estévez, I. (2022, Oct). Validation of a computationally efficient time-domain numerical tool against deepwind experimental data. *Trends in Renewable Energies Offshore*, 597–608. doi: 10.1201/9781003360773-68
- Pribadi, A. B. K. (2024). *Morison additional output*. [https://github.com/abkpribadi/openfast/tree/Morison\\_additional\\_output](https://github.com/abkpribadi/openfast/tree/Morison_additional_output). GitHub. (commit e0bc0cf945afe2559270fbd1c1b33def433a1afc)
- Rappe, V. (2024). (W. De Waele & K. Hectors, Eds.). Retrieved from <https://www.owi-lab.be/sites/default/files/imce/Pages/BEL-Float%20deliverables/BEL.Float.Topic.5-Deliverable.1.pdf>
- Robertson, A., Jonkman, J., Masciola, M., Song, H., Goupee, A., Coulling, A., & Luan, C. (2014, 9). Definition of the semisubmersible floating system for phase ii of oc4. Retrieved from <https://www.osti.gov/biblio/1155123> doi: 10.2172/1155123
- Robertson, A., Jonkman, J., Vorpahl, F., Popko, W., Qvist, J., Frøyd, L., ... Guérinel, M. (2014, 06). *Offshore code comparison collaboration continuation within iea wind task 30: Phase ii results regarding a floating semisubmersible wind system* (Vol. Volume 9B: Ocean Renewable Energy). Retrieved from <https://doi.org/10.1115/OMAE2014-24040> doi: 10.1115/OMAE2014-24040
- Robertson, A. N., Gueydon, S., Bachynski, E., Wang, L., Jonkman, J., Alarcón, D., ... Wohlfahrt-Laymann, S. (2020, sep). Oc6 phase i: Investigating the underprediction of low-frequency hydrodynamic loads and responses of a floating wind turbine. *Journal of Physics: Conference Series*, 1618(3), 032033. Retrieved from <https://dx.doi.org/10.1088/1742-6596/1618/3/032033> doi: 10.1088/1742-6596/1618/3/032033
- Robertson, A. N., Wendt, F., Jonkman, J. M., Popko, W., Dagher, H., Gueydon, S., ... Debruyne, Y. (2017). Oc5 project phase ii: Validation of global loads of the deepwind floating semisubmersible wind turbine. *Energy Procedia*, 137, 38-57. Retrieved from <https://www.sciencedirect.com/science/article/pii/S1876610217352931> doi: <https://doi.org/10.1016/j.egypro.2017.10.333>
- WAMIT, Inc. (2023). *Wamit user manual*. Retrieved from

<https://www.wamit.com/manual.htm>

Wendt, F., Robertson, A., Jonkman, J., & Hayman, G. (2015, 1). Verification of new floating capabilities in fast v8: Preprint. Retrieved from <https://www.osti.gov/biblio/1167453> doi: 10.2514/6.2015-1204